Nano Research
2023, 16(3): 3607–3621

ISSN 1998-0124 CN 11-5974/O4
https://doi.org/10.1007/s12274-022-4319-1

Review Article

Formic acid electro-oxidation: Mechanism and electrocatalysts design

Tongtong Yang[1,2,§], Shuai Hou[1,§], Jiaojiao Xing[1,2], Changpeng Liu[1,2], Junjie Ge[1,2] (✉), and Wei Xing[1,2] (✉)

[1] *State Key Laboratory of Electroanalytical Chemistry, Changchun Institute of Applied Chemistry, Chinese Academy of Sciences, Changchun 130022, China*
[2] *University of Chinese Academy of Sciences, Beijing 100039, China*
[§] *Tongtong Yang and Shuai Hou contributed equally to this work.*

Received: 17 December 2021 / **Revised:** 13 March 2022 / **Accepted:** 13 March 2022

ABSTRACT

As a model reaction for the electrooxidation of many small organic molecules, formic acid electrooxidation (FAEO) has aroused wide concern. The promises of direct formic acid fuel cells (DFAFC) in application further strengthen people's attention to the related research. However, despite decades of study, the FAEO mechanism is still under debate due to the multi-electron and multi-pathway nature of the catalytic process. In this review, the progresses towards understanding the FAEO mechanism along with the developed methodology (electrochemistry, *in-situ* spectroscopy, and theoretical calculation and simulation) are summarized. We especially focused on the construction of anti-poisoning catalysts system based on understanding of the catalytic mechanism, with anti-poisoning catalyst design being systemically summarized. Finally, we provide a brief summarization for current challenges and future prospects towards FAEO study.

KEYWORDS

formic acid electrooxidation, mechanism, anti-poisoning, methodology, *in-situ* technique, electrocatalysts design

1 Introduction

The first and second industrial revolutions have built a modern and prosperous society based on fossil energy, which however also brings about energy crisis and environmental pollution problems [1, 2]. Figures 1(a) and 1(b) show us the dramatically changes of greenhouse gases concentrations and the phenomena of global warming [3]. Driven by the fossil fuel exhaustion, energy security, and climate change, the world's energy composition is being reintegrated [4– 9]. It is suggested that renewable energy will surpass fossil energy in the world's primary energy consumption and become the dominant energy source by 2050 (Fig. 1(c)) [10, 11].

As an efficient and clean energy conversion device, proton exchange membrane fuel cells (PEMFCs) constitute the cornerstone of further renewable energy based society, owing to their simplicity, high power density, and quick start-up features [12– 18]. Various kinds of materials can be used as fuels [19], including methanol, formic acid, hydrogen, ethanol, etc. Among them, tremendous efforts have been devoted to the exploration of direct formic acid fuel cells (DFAFCs), owning to the merits including high fuel safety, high theoretical open circuit potentials (1.48 V), and lower crossover rates through Nafion membranes [20– 26]. As shown in Fig. 2, formic acid can be synthesized from CO_2 and the energy cycling process gives a net carbon neutral feature [27– 33]. Meanwhile, the study of the electro-oxidation mechanism of formic acid is of fundamental significance for revealing the electro-oxidation of many other small organic molecules as formic acid is a common intermediate product [34– 36]. Therefore, in the past fifty years, research on mechanism of formic acid electro oxidation (FAEO) has been a continuous topic of interests.

In this mini review, we summarized how the understanding towards FAEO mechanism evolves with the development of *in-situ* and *operando* techniques, where the current mainstream viewpoints are shared. Meanwhile, the techniques utilized for the mechanism studies, including electrochemistry methods, *in-situ* spectroscopy techniques, and theoretical calculation have been elucidated systematically in detail, hoping to provide inspiration for future FAEO mechanism study. After a series of recent reported FAEO catalysts are discussed, we also provide our perspective towards related reach filed.

2 Reaction mechanism of FAEO

As mentioned above, in spite of the significance of FAEO, its reaction mechanism is still under debate after decades of study. In this section, we firstly review how the understanding of FAEO mechanism evolves with the development of probing tools in related fields. Figure 3 is a brief timeline for FAEO study, where the mechanism is understood gradually from macro to micro, and from coarse to elaborate.

2.1 The evolution process of the mechanism cognition

The earliest studies towards FAEO can be traced back to the 1920s, where Müller and his coworkers were the pioneers for research on FAEO [37– 39]. Herasymenko found the inhibiting

Address correspondence to Junjie Ge, gejj@ciac.ac.cn; Wei Xing, xingei@ciac.ac.cn

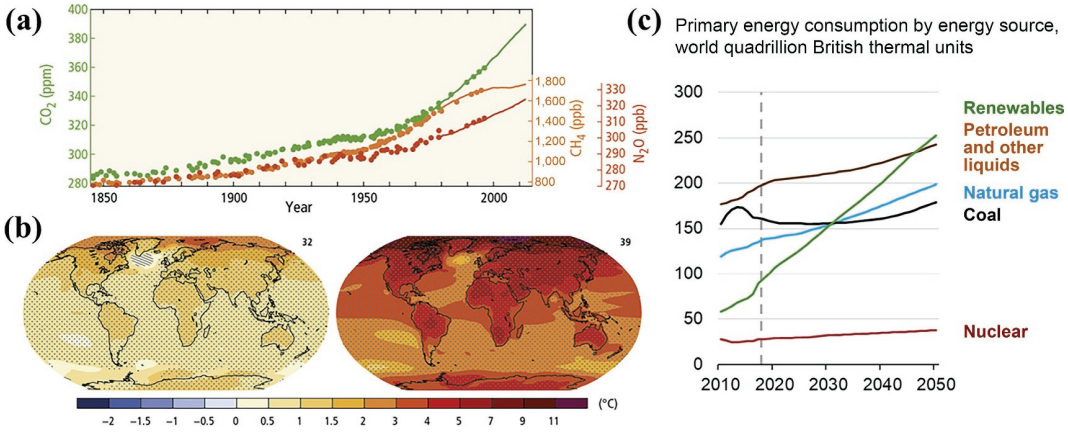

Figure 1 (a) Atmospheric concentrations of the greenhouse gases carbon dioxide (CO_2, green), methane (CH_4, orange), and nitrous oxide (N_2O, red) determined from ice core data (dots) and from direct atmospheric measurements (lines). (b) Change in average surface temperature based on multi-model mean projections for 2081–2100 relative to 1986–2005 under the different scenarios, according to the Fifth Assessment Report (AR5) of the Intergovernmental Panel on Climate Change (IPCC). Reproduced with permission from Ref. [3], © Intergovernmental Panel on Climate Change 2015. (c) Worldwide primary energy consumption by energy source including renewables, petroleum and other liquids, natural gas, and coal. According to the U.S. Energy Information Administration's International Energy Outlook 2019 and 2020 (IEO2019 and IEO2020). Reproduced with permission from Refs. [10, 11], © U.S. Energy Information Administration 2019 and 2020 respectively.

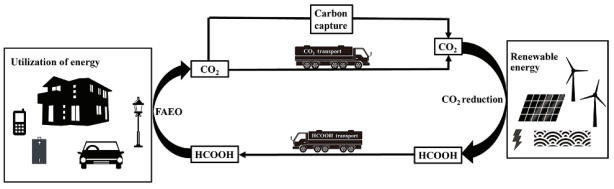

Figure 2 A schematic diagram of carbon-neutral "formic acid economy" with formic acid as the core energy storage substance.

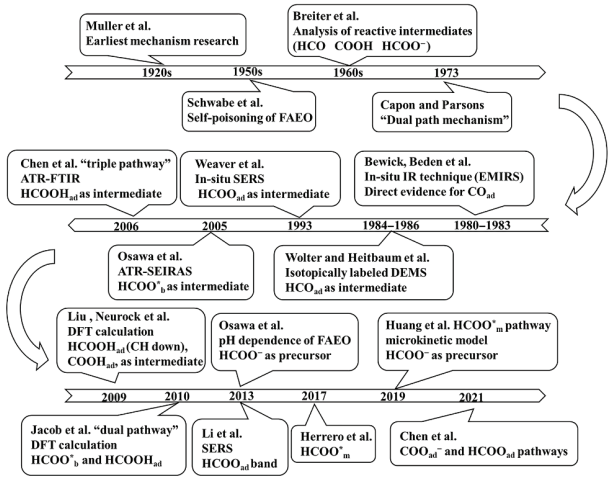

Figure 3 A brief timeline of researches towards FAEO mechanism in the past decades of years.

effect of anion towards the FAEO and he ascribed the limiting current to a postulated nonelectrochemical step or the formic acid oxidation reaction (FAOR) without prior adsorption at high potential [40]. Schwabe discovered a maximum decomposition rate of formic acid at about pH 4.2, where he suggested that HCOOH instead of $HCOO^-$ as the reaction species. He also found the self-poisoning of FAEO but there was no evidence for the existence of postulated monolayer of adsorbed CO [41]. Other work from Buck and Griffith [42], Slott [43], Rhodes and Steigelmann [44], Conway and Dzieciuch [45], and Giner [46] also provided evidences that some adsorbed species poisoned the catalyst. Breiter studied the maximum adsorption from HCOOH solution and the constant adsorbed charge up to about 0.8 V [47, 48]. Brummer studied the relationship between the oxidation rate and electrode preparation, pH, and formic acid concentration [49– 54]. After analysis by gas chromatography, Breiter demonstrated that two electrons are required for the production of one CO_2 molecule [55]. Taylor and his coworkers claimed that the adsorption species was formed at low potentials and it inhibited the oxidization of an active intermediate. He declared that $HCOO^-$ was the electroactive species because of the drastic inhibition of FAEO by Cl^- [56, 57]. After extensive electrochemical research, Capon and Parsons summarized multitudinous work from researchers and proposed the dual path mechanism for FAEO. The generalized mechanism is shown in Eq. (1), the main reaction path follows i_1 and i_3. Although the relation between i_1 and i_2 is uncertain, it is definite that i_4 is very uncommon unless the anode potential is extremely high [58–60].

$$\mathrm{HCOOH} \begin{cases} \xrightarrow{i_1} \text{Reaction surface intermediate} \xrightarrow{i_3} \mathrm{CO_2} \\ \xrightarrow{i_2} \text{Chemisorbed intermediate ("poison")} \xrightarrow{i_4} \mathrm{CO_2} \end{cases} \quad (1)$$

Because of the multifarious reaction paths and adsorbed intermediate species, traditional electrochemical research methods are incapable in elaborating the FAOR reaction mechanism in detail. In order to detect the adsorbed intermediate species at the electrode –electrolyte interface, researchers employed advanced techniques and developed *in-situ* spectroscopy technology [61–65] for mechanistic study. Alan Bewick and his coworkers extended modulated specular reflectance spectroscopy (MSRS) into the true vibrational infrared (IR) region, which is suitable for *in-situ* study of adsorbed species on the electrode interface of aqueous and non-aqueous systems [66–68]. Based on work from Bewick et al., B. Beden developed an *in-situ* spectroscopy technology, called electrochemically modulated infrared reflectance spectroscopy (EMIRS), and they found direct evidence for the presence of bridge-bonded and linearly bonded CO species as poisoning species on the platinum electrode during FAEO process for the first time [69–72].

The successful application of infrared spectroscopy had greatly promoted the mechanistic study [34]. As EMIRS was extensively used for the identification of adsorbates in varied electrochemical conditions (including different electrode potentials, bulk concentrations, and surface structures), several different infrared techniques were also developed [73– 75]. K. Kunimatsu studied how electrode potential influences the formation and oxidation of linearly bonded CO species by polarization modulated infrared reflection-absorption spectroscopy (PMIRS) [76]. Michael J.

Weaver used an alternative potential-difference infrared (PDIR) procedure that employs a signal-potential sweep or step during the Fourier transform data acquisition which was dubbed single-potential alteration infrared spectroscopy (SPAIRS). SPAIRS can be utilized to obtain quantitative information on irreversible potential-induced compositional changes for adsorbates in the thin-layer solution and it can also be coupled directly with simultaneous voltammetric sweep measurements [77– 79]. Inspired by the electrochemical mass spectroscopy (EMS) invented by Bruckenstein [80], O. Wolter and J. Heitbaum reported a method called differential EMS (DEMS), which can be utilized to quantitively study the electrochemical processes via collecting and identifying volatile intermediates [81, 82]. O. Wolter and J. Heitbaum proposed HCO_{ad} as the strongly bound intermediate of formic acid and methanol with the help of isotope-labeled DEMS [83–85].

Molecules adsorbed on metal electrodes under certain conditions exhibit an anomalously large Raman scattering efficiency with high resolution in wide frequency range and low obstruction from surrounding media, which can be used to study the adsorbed species on the electrode surface [86– 88]. Michael J. Weaver studied the electro-oxidation of formic acid under voltammetric conditions on gold and platinum-coated gold electrodes by means of surface enhanced Raman scattering (SERS) and proposed adsorbed formate ($HCOO_{ad}$) rather than CO as reaction intermediate [89– 91]. Zhong-Qun Tian showed convincingly that SERS can be generated on transition metal substrates (e.g., Pt, Ru, Rh, Pd, Fe, Co, Ni, and their alloys) by developing various roughening procedures and optimizing the performance of the confocal Raman microscope [92]. Peigen Cao and his coworkers studied the dissociation and electrooxidation of formic acid at platinum in nonaqueous solutions as probed by *in situ* SERS. They found evidence of linearly bound carbon monoxide on platinum and higher carbon monoxide oxidation activity of rough platinum electrode than smooth platinum electrode [93].

Coming to the 21st century, with the continuous development of characterization techniques such as electrochemical *in-situ* spectroscopy and the application of first-principles *ab initio* calculations, research on FAOR has once again gained extensive attention and some notable progress has been made, as discussed in the next section.

2.2 The proposed mechanisms of FAEO

As stated above, many different explanations towards FAEO mechanisms have been proposed, and we summarize here some of the most prevailing understandings, as shown in Fig. 4. A dual path mechanism was proposed based on traditional electrochemical methods [58– 60]. With the aid of *in-situ* spectroscopy technology, direct evidences for presence of adsorbed (CO_{ad}) and $HCOO_{ad}$ promoted the understanding in reaction mechanism. While CO is regarded as the poisoning species during FAEO, adsorbed formate is a disputed species. Osawa's group suggested the bridge bonded formate ($HCOO_b$) as reactive intermediate [94, 95]. Chen et al. proposed a " triple pathway" mechanism where the oxidation of adsorbed formic acid ($HCOOH_{ad}$) was the dominant direct reaction pathway, and the adsorbed formates acted as reaction blocking spectator species [96, 97]. Theoretical calculations from Neurock et al. also suggested that the adsorbed formates ($HCOO_b$) acted as a spectator, because the subsequent activation barrier of C–H bond is prohibitive [98]. However, Liu et al. proposed that FAEO mainly occurs via the direct oxidation of $HCOOH_{ad}$ (CH-down) and the adsorbed formate is a necessary catalyst [99]. Jacob et al. suggested that the $HCOOH_{ad}$ as a precursor and monodentate formate ($HCOO_m$) and adsorbed CO_2 as intermediate for formate mechanism and direct mechanism towards FAEO [100– 102]. With pH dependent FAEO studied, Osawa et al. proposed that FAEO occurs via a weakly adsorbed $HCOO^-$ precursor [103]. Based on density functional thoery (DFT) calculation research, Herrero et al. proposed that the monodentate formate is the reactive intermediate and the bridge bonded formate acts as a stabilizer [104]. With an integrated view of multifaceted roles of reaction intermediates, Huang et al. proposed two pathways. In his opinion, $HCOO_m$ is the main active intermediate with $HCOO^-$ as the main precursor, and $HCOO_b$ is the site-blocker with HCOOH as the precursor [105]. Recently, Chen et al. proposed a dual-pathway mechanism with both $HCOO_{ad}$ and adsorbed COO^- pathways operating simultaneously with consideration of both pH effect and H/D kinetic isotope effect [106].

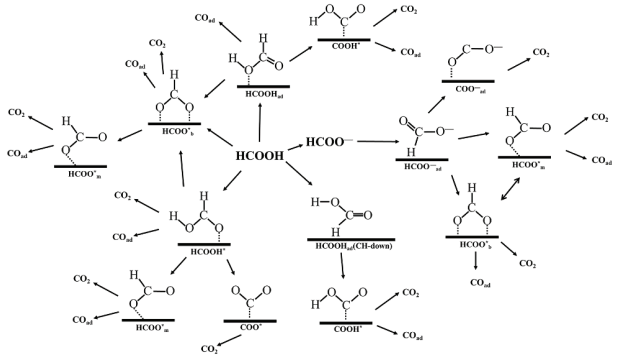

Figure 4 The proposed FAEO mechanisms.

2.3 Mechanisms of CO tolerance catalysts for FAEO

Traditional Pt/C and Pd/C catalysts are not ideal towards FAEO because of the surface blockage caused by produced CO species. Rational design of high performance anti-toxic FAEO catalysts usually follows two principles, to realize the high selectivity of the direct pathway of dehydrogenation and to efficiently oxidize the CO species.

The better anti-toxicity and stability can be realized by manipulating the electronic properties of the active catalytic sites properly. A series of improvements have been made by Ligang Feng and coworkers. They found that the poisoning and stability problem of traditional Pd/C catalyst can be greatly depressed by introducing CoP [107] and Ni_2P [108] owing to the electronic interaction effect from Pd, Ni_2P, and CoP. Younan Xia recently reported that the activity and stability of Pd can be greatly improved when forming a stable hydride phase, $PdH_{0.706}$. Results from both experiments and theoretical calculations indicate that the hydride catalyst has reaction pathway selectivity, since the relative stability of HCOO and COOH intermediates can be modulated [109].

The shape and exposed facets are related to the catalytic performance directly [110– 113]. For example, as one of the best monometallic electrocatalysts for FAEO, palladium nanocrystals with different types of facets and twin defects were thoroughly investigated by Younan Xia and coworkers. They found that the nanocrystals enclosed by (100) facets show higher specific activities than those enclosed by (111) facets. Meanwhile, palladium decahedra and palladium icosahedra exhibited higher specific activities than palladium cubes. It is suggested that the presence of twin defects imposed a stronger impact on the catalytic activity. They ascribed the enhancement in defect region to the increased flux through the formate (HCOO) mediated pathway rather than the carboxyl (COOH) mediated pathway. Since COOH is a precursor to CO and a lower coverage of CO at the defect regions will lead to a higher activity [114].

$$CO + Ru—OH \longrightarrow Ru + CO_2 + H^+ + e^-$$
or
$$COH + Ru—OH \longrightarrow Ru + CO_2 + 2H^+ + e^- \quad (2)$$

The synergistic effect of adjacent catalytic sites also plays an indispensable role for anti-poisoning catalysts. Alloying is the most common way to improve the performance of traditional Pt/C and Pd/C catalysts. A bifunctional mechanism is revealed necessary to promote the oxidation of the intermediate and yield the final product CO_2, as shown in Eq. (2) [115]. Ligang Feng et al. synthesized Pd@CeO_2 with strengthened Pd-O-Ce linkage as efficient FAEO catalyst. With transference of high valence state of Pd^{4+} and metallic Pd into the CeO_2 lattice, efficient FAEO can be realized based on bifunctional mechanism [116]. They also found that PdNi alloy supported on N-doped graphene aerogel (PdNi/GA-N) can realize FAEO over a wide potential range with improved anti-toxicity property. The lower potential for CO oxidation was realized by the bifunctional mechanism with the oxophilicity of Ni [117, 118]. The third-body effect, where the second metal is introduced to segregate the Pt sites and thereby inhibits the CO reaction pathway, is also found useful in the anti-poisoning study. Ezequiel Leiva and his coworkers constructed a theoretical FAOR model to analyze the variation in geometric distribution of adatoms, which showed good agreement with the experimental data of related systems [119]. To date, PtBi, PtSn, PtPb, PtSb, PtCo, PtCu-Mo_2C, and PtRu were investigated extensively, with the anti-poisoning mechanism recognized as bifunctional mechanism or the third-body effect [115, 120–127].

3 Methodology

During the early-stage studies, traditional electrochemical methods can hardly provide direct evidence for the mechanism at molecular level, where researchers have only reached a consensus on the dual-path mechanism. The emergence and development of electrochemical spectroscopy technology enabled the explanation of the mechanism at molecular level. Later, the development of theoretical calculations and simulations accelerated the in-depth understanding. The latest researches tend to combine various advanced technologies to provide more detailed and convincing evidence to comprehensively interpretate the reaction mechanisms. Apparently, the development of new research methodology is the core motivation for mechanism research. In this part, a generally review of different methods applied on the FAEO mechanism investigation will be provided.

3.1 Related *in-situ* spectroscopic techniques

The development and improvement of *in-situ* spectroscopy technology provide direct evidence for poisoning species and reaction intermediates during the FAEO process. In the past decades, electrochemical infrared spectroscopy, SERS, and DEMS provide the main *in-situ* evidence in the FAEO mechanism research.

As mentioned before, the application of EMIRS in FAEO firstly provided conclusive evidence for the existence of CO poisoning species. Figure 5(a) shows the EMIR spectra at different amplitudes of potential modulation at 8.5 Hz for Pt in 0.25 M H_2SO_4 + 0.25 M HCOOH at room temperature. The strong peaks at about 2,055 and 1,840 cm^{-1} belong to linearly bonded CO and multi-bonded CO, respectively. When the pulse amplitude reaches 700 mV, both signals disappear due to the oxidation of the CO species into CO_2 [72]. This technique is sensitive enough to detect relative changes of absorbance of 10^{-4} and it is sufficient to detect sub-monolayer amounts of adsorbed species like CO [34]. Then, the developed SPAIRS extends infrared technology to irreversible electrochemical systems and is coupled with real time voltammetric sweep measurements. With the optimizations of optical alignment and spectroelectrochemical cells, infrared absorption reflection spectroscopy measurement in an attenuated total reflection configuration (ATR-FTIR) is a powerful technique for *in-situ* information collection of electrode –electrolyte

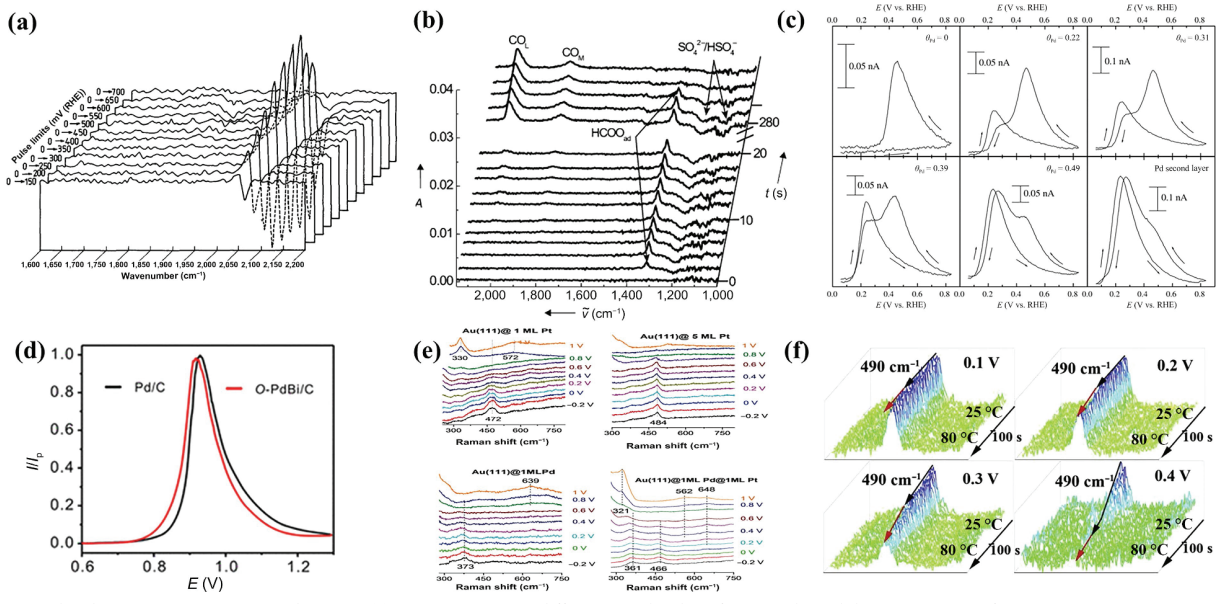

Figure 5 Related *in-situ* spectroscopic techniques. (a) EMIR spectra at different amplitudes of potential modulation at 8.5 Hz for Pt in 0.25 M H_2SO_4 + 0.25 M HCOOH at room temperature. Reproduced with permission from Ref. [72], © Elsevier B.V. 1983. (b) ATR-FTIR result for FAEO on a Pt thin film electrode. Reproduced with permission from Ref. [96], © Wiley-VCH Verlag GmbH & Co. KGaA, Weinheim 2006. (c) DEMS information of CO_2 (m/z = 44) obtained from Pt(100) with different palladium coverage values with applied potential in 0.25 M HCOOH + 0.5 M H_2SO_4 solution. Reproduced with permission from Ref. [128], © Springer 2006. (d) DEMS signals of CO_2 during CO stripping voltammograms on Pd/C and O-PdBi/C (PdBi ordered intermetallic) electrode. Reproduced with permission from Ref. [129], © American Chemical Society 2020. (e) SHINERS information of CO electrooxidation on different electrodes in 0.1 M $HClO_4$ saturated CO. Reproduced with permission from Ref. [130], © Wiley-VCH Verlag GmbH & Co. KGaA, Weinheim 2018. (f) Time-dependent SERS spectra recorded on Au@Pt/TCME (thermocouple microelectrode) in 0.5 M H_2SO_4 + 0.05 M HCOOH solution at different temperatures. Reproduced with permission from Ref. [131], © Elsevier Ltd. 2018.

interface which has high signal-to-noise ratio and sufficient mass transportation [35, 132, 133]. Figure 5(b) presents ATR-FTIR spectra for FAEO on a Pt thin film electrode. The transient experiments were proceeded under continuous electrolyte flow at a constant potential of 0.5 V. The electrolyte flow was changed from pure base electrolyte to formic acid containing electrolyte at t = 0 min and changed back at t = 4.5 min after reaching steady-state. After analyzing the time-varying integrated intensities of the IR signals under different adsorption potentials, more quantitative information will be available [96].

Traditional electrochemistry and spectroscopic techniques are usually limited by the lack of identifying the specific structure of intermediate. DEMS is a powerful *in-situ* technique which allows the near-instantaneous structure detection of volatile and gaseous chemical species and it can be coupled with isotope labeling technology. However, DEMS can only probe volatile and gaseous products and cannot probe the electrode interface intermediate species and precise quantification is also a big challenge [83, 134–138]. Figure 5(c) shows DEMS information of CO_2 (m/z = 44) obtained from Pt(100) with different palladium coverage values with applied potential in 0.25 M HCOOH + 0.5 M H_2SO_4 solution, combined with voltammetric data, the details of formic acid oxidation on these electrodes can be analyzed [128]. Figure 5(d) illustrates DEMS signals of CO_2 during CO stripping voltammograms on Pd/C and O-PdBi/C (PdBi ordered intermetallic) electrode, which resolves the attribution of the oxidation peak and indicates that it is more facile for O-PdBi/C to desorb the adsorbed CO with a lower onset potential [129].

SERS effect was first discovered in mid-1970s, with the ability of providing non-destructive and ultra-sensitive characterization of molecular level information on electrode surface. This technique was placed with great expectations for characterizing the intermediate species at the electrode –electrolyte interface [87, 89– 91, 136, 139, 140]. However, during a long period, SERS was severely limited by finite numbers of optional metals (Ag, Au, and Cu) and strict requirements for surface morphology. Researchers have made long lasting efforts to expand the application of this technology to a universal electrochemical system. There are mainly two methods to improve the SERS effect, surface roughening, and " intensity-borrowing" strategy (introducing external interference into the system, usually Au relevant system) [140]. By developing various roughening procedures and optimizing the performance of the confocal Raman microscope, the SERS effect has been generated on many transition metals and alloys [92]. Xiao Li and coworkers conducted an *in-situ* surface-enhanced Raman spectroscopic research of FAEO on the surface of spontaneously deposited platinum on gold. They first detected a surface formate band at ca. 300 cm^{-1} and ascribed that to the adsorbed formate with an orientation configuration [141]. Tip-enhanced Raman spectroscopy and shell-isolated nanoparticle-enhanced Raman spectroscopy (SHINERS) are notable advanced SERS techniques developed by intensity-borrowing strategy. SHINERS technique invented by Jian Feng Li et al. significantly expanded and optimized the application of SERS. It can be applied to investigate the electronic structures of Pd and Pt layers on Au single crystals. Compared with bulk metals, the interfacial effects of monolayer Pd or Pt covered Au single crystals can weaken the adsorption of CO, leading to a higher activity towards the oxidation of methanol or formic acid [130, 142]. Jing Tang et al. combined SERS and high-frequency heating technology to investigate how FAEO varies with temperatures. They found that the intensity of the Pt-C band drops with an increase in temperature, which indicates that the oxidative desorption of CO from the Pt surface is more favorable at higher temperature [131]. However, the combination of *in-situ* SERS and electrochemical system still needs to be improved, with core issue remain as how to minimize the influence of mass transport, selectivity, reactivity, reactive site, and so on, while achieving significant SERS effect [140, 142, 143]. Figure 5(e) is an example of SHINERS information of CO electrooxidation in 0.1 M $HClO_4$ saturated by CO. By comparing the detailed fingerprint information, information about the surface interaction of catalysts with adsorbed CO molecule, the adsorption of reactive oxygen, and synergistic effects contributing to the higher catalytic activity can be obtained conveniently [130]. Figure 5(f) presents the time-dependent SERS spectra recorded on Au@Pt/TCME (thermocouple microelectrode) in 0.5 M H_2SO_4 + 0.05 M HCOOH solution at different temperatures, which indicates that heating is beneficial to the oxidation and desorption of CO and the oxidation potential plays a decisive role [131].

3.2 Theoretical calculations and simulations

Ab initio quantum mechanical calculation based on first principles is becoming more and more popular to offer complementary information for electrocatalytic system in atomic as well as electronic structure level. It is still a big challenge to construct a theoretical calculation simulation system that can effectively simulate the real electrochemical systems which accounts for the comprehensive consideration of solvent effects, electrolytes, applied potentials, and so on.

Nevertheless, some meaningful results have been obtained by theoretical calculations [144– 149]. Timo Jacob's team demonstrated that different theoretical solvent models result in quite different FAEO mechanism pathways. A constructed model of water bilayer structure on Pt(111) with two different HCOOH configurations is shown in Fig. 6(a), each HCOOH molecule couples with two H_2O molecule which fits in the H-bonding network spanning the entire unit cell. Based on the model with Langmuir –Hinshelwood mechanism, the minimum energy pathway (MEP) corresponds to the formate reaction pathways and the next lowest energy process is a direct pathway involving the COOH* intermediate, as shown in Fig. 6(a) [101, 102]. Figure 6(b) comes from a work from Hui-Fang Wang and Zhi-Pan Liu, a continuum solvation model with a smooth dielectric function implemented in the framework of the periodic DFT calculations which includes both the first solvation shell of water and the rest of the water environment represented by the implicit continuum solvation model. Adsorbed HCOOH-$(H_2O)_4$ with O-down and CH-down configuration, adsorbed monodentate and bidentate HCOO-$(H_2O)_4$, as well as related transient states were finely constructed. Results indicate that the presence of adsorbed formate disrupts the H-bonding network of water at the water/metal interfaces, which further benefits the adsorption of formic acid in the CH-down configuration by reducing the solvation energy loss of formic acid moving from the bulk solution to the metal surface [99]. It is obvious that the adjacent adsorbed species is essential for determining the reaction path for FAEO [100]. Figure 6(c) is another example from E. Herrero's group. They suggest that the monodentate and the bidentate adsorption formate are relevant. The C–H cleavage of monodentate adsorbed formate inside a pocket of preadsorbed bidentate formate on the Pt(100) surface is virtually without barrier [104]. The information of the electronic structure obtained by theoretical calculations is also of great significance for explanation of the reaction mechanism. Figure 6(d) presents the different charge density for the stable adsorption configurations of trans-COOH intermediate on Pd-decorated Cu bimetallic surfaces. The stronger charge transfer between H atom and the surface indicates that Pd_6Cu_3 and Pd_9Cu_0 are more favorable for the cleavage of the O–H bond which coincides

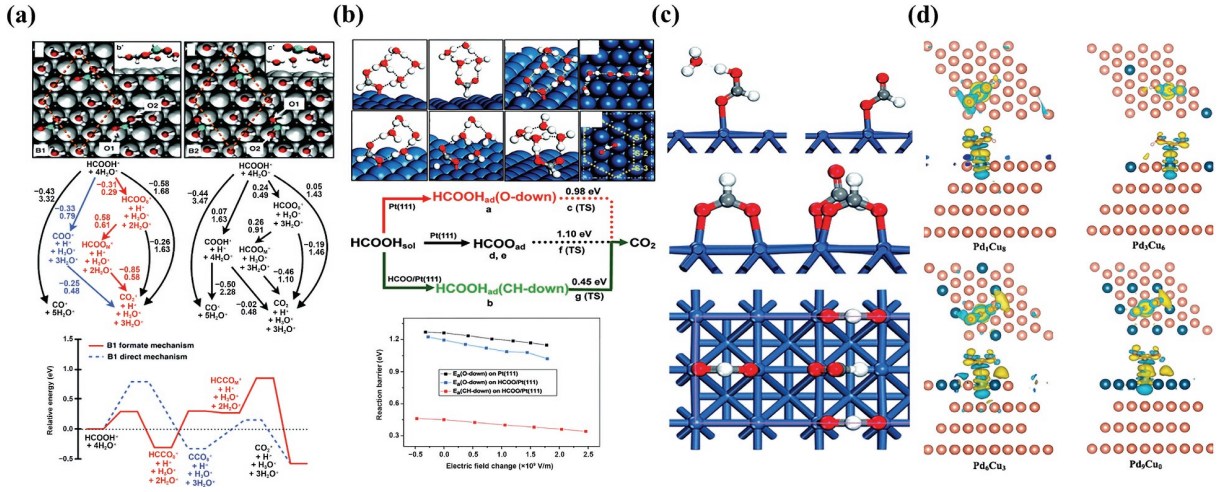

Figure 6 Theoretical calculations and simulations. (a) The lowest energy pathway of Langmuir–Hinshelwood HCOOH oxidation reaction mechanisms with water bilayer structure on Pt(111) with two different HCOOH configurations. Reproduced with permission from Ref. [101], © American Chemical Society 2010. (b) DFT optimized structures for key adsorbed states including $HCOO_{ad}$ and $HCOOH_{ad}$ with O-down and CH-down configurations and energy analysis of related pathways. Reproduced with permission from Ref. [99], © American Chemical Society 2009. (c) Adsorbed formate and solvation model, monodentate adsorbed formate inside a pocket of preadsorbed bidentate formate on the Pt(100) surface. Reproduced with permission from Ref. [104], © The Royal Society of Chemistry 2017. (d) Difference charge density for the stable adsorption configurations of trans-COOH intermediate on Pd-decorated Cu bimetallic surfaces. Reproduced with permission from Ref. [150], © Elsevier B.V. 2020.

with the suggested Pd ensemble effect for direct FAEO mechanism [150].

4 Electrocatalysts for FAEO

Ideal electrocatalysts for FAEO are the foundation of the extensive application of formic acid based energy system. Same as the mechanism research, the exploration of advanced catalysts has never stopped. The ideal electrocatalysts require high electrocatalytic activity as well as low cost, high stability, innocuous, and so on. Herein we introduce a few recent developed catalysts based on some common strategies, and the strategies are brought together to give enhanced performance from time to time.

4.1 Doping

As traditional electrocatalysts for FAEO, platinum and palladium-based materials are the most extensively studied catalysts. By introducing new elements and regulating the electronic and geometry structure of the catalyst, the catalytic performance can be effectively improved. Doping elements include H [20, 109], B [151], P [152], Cu [153], Bi [129, 154, 155], Fe [156], Co [157, 158], Sn [159], W, Cr [160], Au [161–163], Ru [164], and so on.

Zhaoxiong Xie's group reported an improved PdH_X nanocatalyst by simply treating the commercial Pd black with n-butylamine in solvothermal condition. The structure of as prepared PdH_X was confirmed by high-resolution transmission electron microscopy (HRTEM) image and powder X-ray diffraction (PXRD) pattern. The results show that there is an expansion of Pd lattice and the H:Pd ratio is estimated to be 0.43. With the study of valence band structure by X-ray photoelectron spectroscopy (XPS), the structure of the catalyst was confirmed as β-$PdH_{0.43}$. Compared with the commercial Pd black, the prepared $PdH_{0.43}$ exhibited an extraordinarily low peak potential and a high mass activity as shown in Fig. 7(a). The *in-situ* ATR-FTIR spectra in Fig. 7(b) suggest that the FAEO process on this catalyst involves both dehydrogenation and dehydration pathways. Further experiments (Fig. 7(c)) in CO electrooxidation indicated that CO binds to PdH_X less strongly than on commercial Pd black, which is consistent with the d band center theory [20, 165, 166]. Zewei Quan's group reported intermetallic PtSnBi nanoplates with controllable compositions, which were fabricated delicately by sequential complexing-reducing-ordering processes. The as prepared atomically ordered $Pt_{45}Sn_{25}Bi_{30}$ nanoplates show a super high mass activity of 4,394 $mA{\cdot}mg_{Pt}^{-1}$ at 0.4 V, which is 6/39/39 times greater than that of PtBi nanoplates/PtSn nanoparticles/commercial Pt/C as presented in Fig. 7(d). The great improvement of ternary composition over binary composition indicates the synergism of the three component metals. The atomically ordered structure was confirmed by XRD pattern, TEM and aberration-corrected high-angle annular dark field scanning TEM (HAADF-STEM) images, and energy-dispersive X-ray (EDX) maps. CO-stripping curves of intermetallic PtSnBi nanoplates show that the peak potentials are positively shifted and the onset potentials are negatively shifted. They ascribed this phenomenon to the function of Sn, which can react with H_2O to form Sn-OH_{ads} at low overpotential, while the high FAOR activity comes from the enhanced selectivity of direct oxidation of HCOOH. Furthermore, DFT calculation was carried out, as shown in Fig. 7(e), the FAOR activity originates mainly from the optimized direct oxidation pathway through two dehydrogenation steps (HCOOH to HCOO* and HCOO* to CO_2) and the inhabitation of the dehydration path [159]. Figures 7(f) and 7(g) are TEM and HAADF-STEM images with corresponding EDX elemental mappings from a work of Chang Ming Li's team, where they synthesized a layered and heterostructured Pd/PdWCr nanosheet-assembled flower shaped catalyst (L-Pd/PdWCr) based on a facile wet chemical approach. The prepared catalyst has a strong and broad anode catalytic peak with a higher peak current density and a more negative onset potential as illustrated in Fig. 7(h). Based on the Nyquist plots and XPS spectra of Pd_{3d}, they proposed that the superior catalytic activity and stability originated from the novel architecture and the doped W and Cr, which results in fast charge transfer rate, enhanced mass transport channels, promoted dehydrogenation pathway, as well as enhanced stability [160].

Based on traditional Pt and Pd electrocatalysts, the introduction of new doping elements can modulate the electronic and geometry structure of catalytically active sites. As one of the most facile and common strategies, there is still a lack of regularized and systematic cognition. Meanwhile the improvement of catalytic activity is also unsatisfactory.

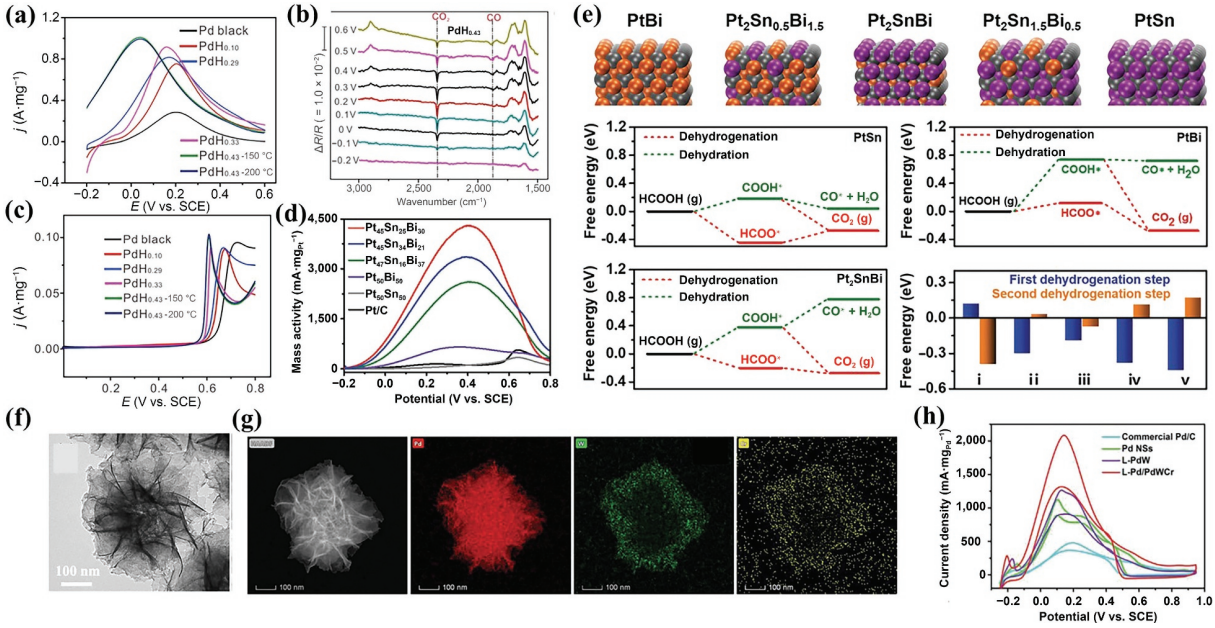

Figure 7 (a) Positive going scan of formic acid electrooxidation on Pd black and PdH_X nanocatalysts with different H contents in 0.25 M HCOOH + 0.5 M H_2SO_4 (scan rate: 50 mV·s^{-1}). (b) *In-situ* ATR-FTIR spectra of FAEO on $PdH_{0.43}$ in 0.25 M HCOOH + 0.5 M H_2SO_4 solution at different potentials, which were varied from –0.20 to 0.60 V. (c) CO electrooxidation on Pd black and PdH_X nanocatalysts in 0.5 M H_2SO_4 (scan rate: 10 mV·s^{-1}). Reproduced with permission from Ref. [20], © Elsevier Ltd. 2017. (d) Anodic scan polarization curves of different PtSnBi nanoplates catalysts toward FAOR recorded at a scan rate of 50 mV·s^{-1} in Ar-saturated 0.5 M H_2SO_4 + 1 M HCOOH electrolyte. (e) DFT calculation of FAEO on different PtSnBi nanoplates including dehydrogenation and dehydration pathways. Reproduced with permission from Ref. [159], © WILEY-VCH Verlag GmbH & Co. KGaA, Weinheim 2019. (f) and (g) TEM and HAADF-STEM images of L-Pd/PdWCr and the corresponding EDX elemental distribution of Pd, W, and Cr. (h) CV curves of the commercial Pd/C, Pd NSs, L-PdW, and L-Pd/PdWCr in 0.5 M H_2SO_4 + 0.5 M HCOOH electrolytes. Reproduced with permission from Ref. [160], © Wiley-VCH GmbH 2020.

4.2 Coordination environment control of catalytic center

The metal–support interaction can also significantly affect the catalytic behavior of the noble catalysts towards FAOR by electronic structure modulation, among which the metal oxides and a wide range of carbon-based materials were used [26, 151, 167–172]. Juan Wang et al. reported the highly dispersed Pd nanoparticles (~ 3.6 nm) supported on boron-doped graphene/graphitic carbon nitride (Pd/BG-CN) three-dimensional (3D) hybrids as efficient FAEO catalyst. The 3D BG-CN hybrid was synthesized by a procedure involving sonication, rotary evaporation, hydrothermal treatment, lyophilization, and thermal polycondensation. Pd nanoparticles were deposited onto BG-CN by an impregnation-reduction method. Scanning electron microscopy (SEM) and HRTEM results in Figs. 8(a) and 8(b) revealed that the nanosheet surface was covered with small particles. Based on the XPS survey pattern of the Pd 3d spectra in Fig. 8(c), Pd/BG-CN had a much higher Pd^0 content than that of prepared Pd/G. Pd nanoparticles were stabilized through their strong interactions with the B and N heteroatoms. According to the electrochemical test, Pd/BG-CN exhibited excellent FAEO activity superior to commercial Pd/C and other reported Pd-based catalysts (Fig. 8(d)). They ascribe the efficient utilization of active Pd, the electronic effect and structural contribution of the BG-CN support [151]. Hyunjoo Lee et al. prepared high load (8 wt.%) Pt single atom catalyst supported on antimony-doped tin oxide (Pt1/ATO) by conventional incipient wetness impregnation. HAADF-STEM images (Figs. 8(e) and 8(f)) and theoretical calculation results indicated that the Pt atoms can be stabilized by substituting the SnSb and SnO_2 surface array lattice atoms. The extended X-ray absorption fine structure (EXAFS) results (Fig. 8(g)) confirmed the single-atomically dispersed platinum. The electronic structure of Pt was evaluated by X-ray absorption near edge structure (XANES) and XPS, which showed electron transfer from ATO to Pt. Electrochemical test suggested that Pt1/ATO exhibited high activity, selectivity, and durability towards FAEO in direct pathway (Fig. 8(h)). The super high atom utilization results in an order of magnitude higher mass activity than Pt/C [167]. Yadong Li et al. synthesized efficient Ir_1/CN FAEO catalyst by a general host –guest strategy, where zeolite imidazolate framework 8 (ZIF-8) was chosen as the host and iridium acetylacetonate ($Ir(acac)_3$) as the guest. The atomic dispersion of Ir was confirmed by high-resolution HAADF-STEM image and Fourier-transformed (FT)-EXAFS analysis (Figs. 8(i) and 8(j)). The average oxidation number of iridium species indicated from XANES was 2.42, which was consistent with XPS measurement. A DFT calculation was carried out to investigate the FAOR mechanism (Fig. 8(k)) and a highly reactive FAOR process through a direct pathway of COOH* without the formation of poisonous CO was suggested. The Ir-N_4 coordination structure was confirmed by DFT calculation and XANES spectrum simulation. Electrochemical test suggested that Ir_1/CN not only has high activity towards FAEO (Fig. 8(l)), but also shows high CO resistance. *In-situ* XAFS measurements presented a trend where the average oxidation number of iridium decreased with the increase of current density. It can be ascribed to the electron transfer from formic acid to iridium during the FAOR [168].

Local coordination environment of catalytic center is directly related to the activity. With precise control of the coordination environment of active catalytic center, efficient selectivity and high activity can be successfully achieved. Although it is still challengeable to realize accurate synthesis and characterization of coordination environments.

4.3 Morphology regulation

Optimizing the morphology is also necessary for further advancing the catalysts, which influences both stability and efficiency of the catalytic sites. A large number of reports on catalysts with different morphologies were reported, including nanoplates [153, 154, 159], nanorods [152, 173], core–shell [156, 171, 174], nanotubes [175], nanocubes (NCs) [176], nanoflowers [151, 160], nanospines [164], nanostrings [169], nanoframes [177],

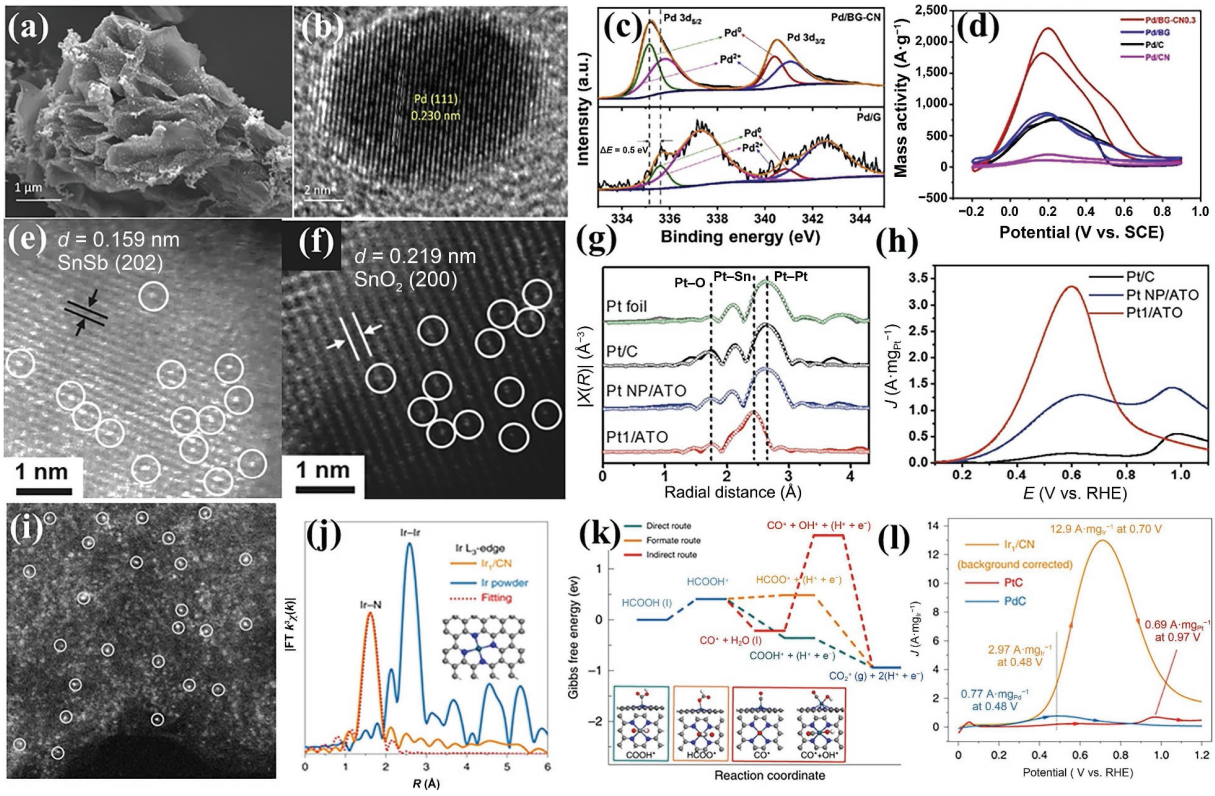

Figure 8 (a) and (b) SEM and HRTEM images of Pd/BG-CN. (c) XPS high resolution regions of Pd 3d for Pd/G and Pd/BG-CN . (d) CV curves of catalysts in N_2-saturated 0.5 M H_2SO_4 +0.5 M formic acid at a scan rate of 50 mV·s^{-1}. Reproduced with permission from Ref. [151], © Elsevier B.V. 2019. (e) and (f) HAADF-STEM images of Pt1/ATO. (g) EXAFS (line: measured, symbol: fitted) data for Pt foil, reduced Pt/C, Pt NPs/ATO, and Pt1/ATO samples. (h) FAOR forward scans in Ar-saturated 0.1 M $HClO_4$ with 0.5 M HCOOH solution. Reproduced with permission from Ref. [167], © WILEY-VCH Verlag GmbH & Co. KGaA, Weinheim 2017. (i) High-resolution HAADF-STEM image of Ir_1/CN. (j) FT-EXAFS spectra of Ir_1/CN and iridium powder at the iridium L_3-edge. (k) DFT calculation of FAEO on Ir_1/CN and related Gibbs free energy diagram. (l) Forward-scan voltammetric curves of Ir_1/CN, commercial Pd/C, and commercial Pt/C in 0.5 M H_2SO_4/0.5 M HCOOH at a scanning rate of 50 mV·s^{-1}. Reproduced with permission from Ref. [168], © Li, Z. et al. 2020.

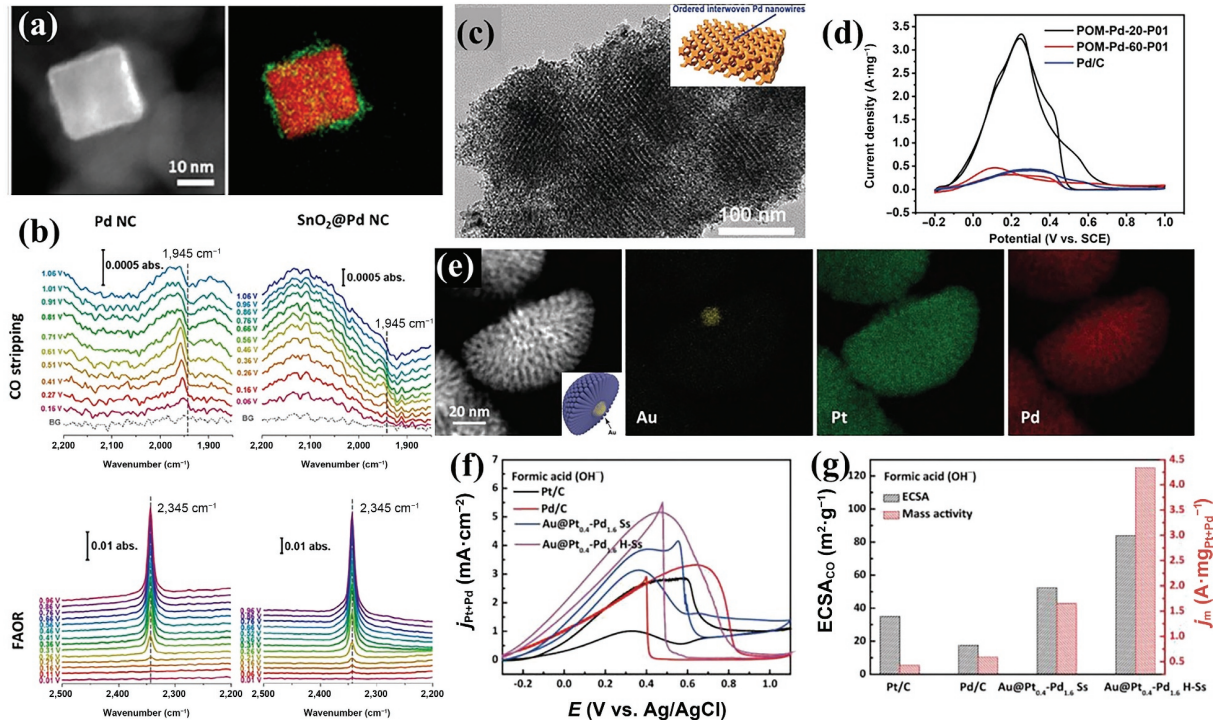

Figure 9 (a) HAADF-STEM image and EDX mapping of SnO_2@Pd NCs. (b) *In-situ* FTIR of the CO-stripping and FAEO of Pd NCs and SnO_2@Pd NCs. Reproduced with permission from Ref. [176], © American Chemical Society 2020. (c) TEM image of the POM-Pd-20-P01 sample (POM-Pd-*m*-P/N*n*, *m* and *n* are the temperature and potential values, and P/N are short for positive/negative potential). (d) CV curves of POM-Pd-20-P01, POM-Pd-60-P01, and Pd/C samples in 0.5 M H_2SO_4 + 0.5 M HCOOH at 50 mV·s^{-1}. Reproduced with permission from Ref. [178], © Wiley-VCH Verlag GmbH & Co. KGaA, Weinheim 2019. (e) HAADF-STEM image and the corresponding EDX elemental mapping analysis of Au (yellow), Pt (green), and Pd (red) contents in Au@Pt–Pd H-Ss. (f) CV curves in 1.0 M KOH aqueous solution containing 1 M formic acid at scan rate of 50 mV·s^{-1}. (g) Comparison of $ECSA_{CO}$ and FAOR mass activity of the commercial Pt/C catalyst, commercial Pd/C catalyst, Au@$Pt_{0.4}$-$Pd_{1.6}$ Ss, and Au@$Pt_{0.4}$-$Pd_{1.6}$ H-Ss. Reproduced with permission from Ref. [174], © Wiley-VCH GmbH 2021.

and so on [178, 179].

Beatriz Roldan Cuenya's group synthesized SnO_2@Pd NCs (Fig. 9(a)) by hydrothermal method. The quasi *in-situ* XPS and *operando* XAFS characterization revealed that the chemical state of SnO_2 and reduced state Pd^0 had not changed after electrochemical test. The structure of SnO_2@Pd nanocubes was stabilized by the presence of SnO_2. Electrochemical analysis suggested that the presence of Sn could facilitate the oxidative removal of CO and enhance the catalytic activity. It was also confirmed by *in-situ* FTIR of CO-stripping and FAEO experiments as shown in Fig. 9(b) [176]. Cheng Zhong et al. prepared palladium membranes with periodically ordered mesoporosity (POM-Pd) by a lyotropic liquid-crystal (LLC) templated electrodeposition procedure. To progressively optimize configuration of microporosity, POM-Pd-20-P01 samples (POM-Pd-*m*-P/N*n*, *m* and *n* are the temperature and potential values, and P/N are short for positive/negative potential.) with variable thicknesses were prepared (Fig. 9(c)). The POM-Pd-20-P01 sample delivers a peak gravimetric current density of 3.34 $A \cdot mg^{-1}$ for the FAOR, which is 7.1 and 7.8 times than that of POM-Pd-60-P01 and Pd/C, respectively (Fig. 9(d)). Through the electrochemical test, they found that the area specific activity increased nearly linearly with increase in electrochemically active surface areas (ECSA), regardless of mass loading, which proved the excellent accessibility of the mesopores as well as the facile mass transport kinetics. Further comparative tests proved that the configuration of porosity is of more vitally importance instead of ESCA. FAEO experiment suggests the direct oxidation mechanism of HCOOH into CO_2 without CO intermediate and the superiority of catalytic activity among the-state-of-the-art Pd-based catalysts [178]. Lin Jiang et al. prepared 3D Au@Pt-Pd hemispherical nanostructures (Au@Pt-Pd H-Ss) with both element distribution and morphological anisotropy (Fig. 9(e)) which exhibit superior electrocatalytic activity and durability for methanol, ethanol, and formic acid oxidation reaction. The random adsorption of BO_2^- on Au seed surface showed a vital influence on the formation of anisotropic hemispherical nanostructure. DFT calculation results suggest that with BO_2^- decoration, the formation of Pt–Pd atoms on Au seed will be much more thermodynamically feasible. The superior electrooxidation activity towards methanol, ethanol, and formic acid under alkaline conditions was confirmed by a series of electrochemical tests (Fig. 9(f)). The advanced structure of Au@Pt-Pd H-Ss results in the improved mass activity, ECSA, and outstanding stability (Fig. 9(g)) [174].

Rational design of morphology is a necessary condition for realizing excellent catalysts. The design strategy is focused on large surface area with abundant active sites, good conductivity, and mass transfer.

4.4 Size effect

A large number of studies have now shown that catalyst size reduction is not only crucial for increasing the metal atom utilization, but also strongly alters the electronic structure (Fig. 10(a)). Nevertheless, a unified theory that can explain and predict the catalytic behavior of various sized catalysts (single atoms [167, 168, 180], nanoclusters [162, 181, 182, 183], and nanoparticles [129, 157, 165, 170, 184]) towards different reactions is still in the exploratory stage [185].

Peng Zhang et al. synthesized a series of PtAu nanoparticles with tailored surface structures and particle diameters on the order of 7 nm by a facile colloidal method. They ascribed the superior FAEO activity to the dehydrogenation pathway selectivity and CO poisoning resistance of Au decorated single Pt site which was confirmed by further electrochemical analysis and DFT calculation (Fig. 10(b)). Cyclic voltammetry (CV) studies showed that the nanoparticles with low Pt content had superior FAEO activity (Fig. 10(c)). Further analysis suggested that the

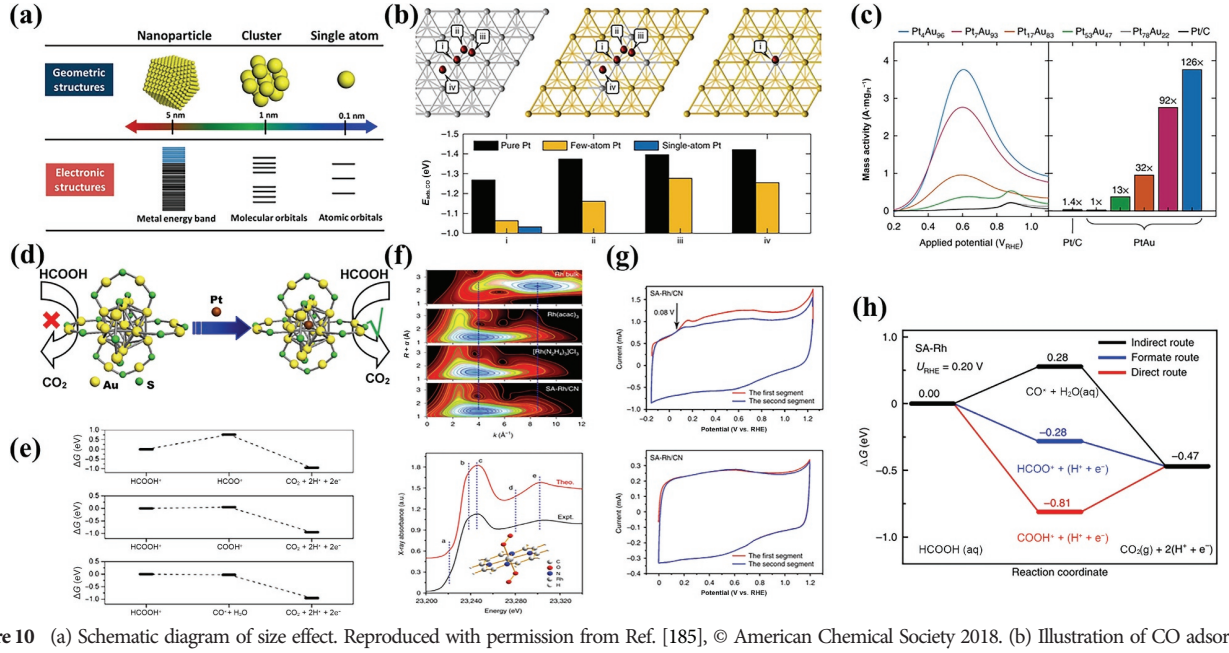

Figure 10 (a) Schematic diagram of size effect. Reproduced with permission from Ref. [185], © American Chemical Society 2018. (b) Illustration of CO adsorption modes on model(111) lattices of pure, few-atom, and single-atom Pt surfaces that shows four different coordination sites (apical, bridging, hexagonal close-packed hollow, and face-centred cubic hollow) and related CO adsorption energies. (c) Pt mass-normalized anodic sweeps obtained from PtAu nanoparticles and commercial Pt/C catalysts in an electrolyte that contained 0.1 M $HClO_4$ + 0.1 M HCOOH and the comparation of peak currents. Reproduced with permission from Ref. [184], © Duchesne, P. N. et al 2018. (d) Illustration of the fabrication of single Pt atom-doped Au_{25} ($Pt_1Au_{24}(SR)_{18}$) NCs for FAEO. (e) Potential dependent free energy diagrams for FAEO on $Pt_1Au_{24}^0$ at the calculated onset potential 0.31 V. Reproduced with permission from Ref. [181], © Elsevier Ltd. 2018. (f) Wavelet transforms for the k^2-weighted EXAFS signals of SA-Rh/CN and reference samples. Comparison between the experimental Rh K-edge XANES spectrum of SA-Rh/CN and the theoretical spectrum calculated for the depicted structure. (g) Two CO stripping experiment for SA-Rh/CN (in 0.5 M H_2SO_4 CO-saturated aqueous solution and 0.5 M H_2SO_4 + 0.5 M HCOOH aqueous solution/0.5 M H_2SO_4 aqueous N_2-saturated solution). (h) Free energy profiles of FAEO via indirect, formate and direct routes on the SA-Rh site at a constant potential of 0.20 V. Reproduced with permission from Ref. [180], © Xiong, Y. et al, 2020.

nanoparticles were Pt surface enrichment and the Pt atoms in Pt_7Au_{93} and Pt_4Au_{96} present almost exclusively as single-atom sites surrounded by atoms of Au [184]. Wei Chen reported single Pt atom doped $Pt_1Au_{24}(SC_{12}H_{25})_{18}$ (named as Pt_1Au_{24}) nanoclusters with significantly enhanced FAEO catalytic activity (Fig. 10(d)). Successfully prepared Pt_1Au_{24} was confirmed by ultraviolet–visible (UV–Vis) absorption spectrum and Matrix-assisted laser desorption ionization-time-of-flight (MALDI-TOF) mass spectrometry. Electrochemical test results verified the high activity, stability, and CO tolerance of the catalyst. DFT calculation results were consistent with experiments and suggested a direct pathway of FAEO with COOH* as the reactive intermediate (Fig. 10(e)) [181]. Yadong Li and coworkers found that single-atom Rh anchored on N-doped carbon (SA-Rh/CN) exhibited an unexpected catalytic performance for FAEO. The catalyst was synthesized via a host –guest strategy. Structure characterization results suggested the homogeneous distribution of $Rh(acac)_3$ in ZIF-8 single rhombic dodecahedron. Further EXAFS and XANES analyses (Fig. 10(f)) confirmed the mononuclear dispersion of the Rh species with distorted octahedral coordination of four N atoms and two axial O atoms. Electrochemical test confirmed that the SA-Rh/CN electrocatalyst exhibits excellent mass activity, 28- and 67-fold higher than that of state-of-the-art Pd/C and Pt/C. Two different CO-stripping experiments (Fig. 10(g)) indicated that SA-Rh/CN can oxidize CO* at a very low potential (0.08 V) and formic acid was oxidize towards direct dehydrogenation. DFT calculation results confirmed the conclusions and suggested that FAEO occurred towards both formate and direct routes (Fig. 10(h)) [180].

Novel kinds of catalysts emerged as single atom, nanoclusters, and nanoparticles have already been extensively studied. With their unique electronic structure as well as geometric structure, the catalytic effect and design strategy are quite different. The main challenge in the future will focus on the controllable atomic synthesis and mechanism exploration [186].

5 Conclusion and perspective

As a model reaction of electro-oxidation of small molecules and an outstanding energy substance, the study of FAEO is of great significance. In the past decades, considerable progress has been made in the research towards mechanism and electrocatalysts design of FAEO. The advances in *in-situ* and *operando* characterization tools, such as ATR-FTIR, DEMS, and SERS, are the internal driving force to a clearer understanding towards FAEO. However, because of the complexity of the electrocatalytic process and electrode interface environment the current *in-situ* technologies are still unable to provide full and absolutely correct information for the mechanistic understanding. Further development in high-resolution and ultrafast *in-situ* characterization techniques suitable for electrode interface researches is essential for future study. The strict requirements of different *in-situ* characterization methods for experimental conditions and the limitations of reaction conditions make it difficult to unify the final interpretation. Further refinement and improvement of *in-situ* characterization techniques are necessary conditions for a clear mechanism explanation. Besides, to reveal the FAEO mechanism comprehensively and accurately, the application of multiple technologies including electrochemical methods, *in-situ* spectroscopy techniques, theoretical calculations, and simulations, is necessitated. Considering the differences in experimental conditions of different *in-situ* characterization techniques, and with the supplement of theoretical calculations and simulation techniques, it is hoped that the closest mechanism explanation can be obtained.

The rational catalyst design is also highly important, a complex combination of factors, including activity, safety, stability, and cost needs to be considered, in order to fully push the real world application of the DFAFC. Combining catalytic material design and catalytic mechanism to adjust FAEO reaction kinetics and thermodynamic processes is the universal catalysts design concept. The ideal catalysts require selective to the FAEO dehydrogenation pathway and tolerant to CO poisoning species. Most FAEO catalysts design is based on the optimization of traditional Pt and Pd catalysts, including doping, loading, and morphology construction. A regular structure –activity relationships need to be further explored. Besides, theoretical calculations can not only help explain the catalytic mechanism, but also help design and optimize the catalytic system. By constructing and optimizing theoretical models, including active site design, interface control, calculation descriptor, excellent catalysts are likely to be quickly screened out [187]. It is worth mentioning that the recently developed high-performance single-atom catalysts with precise design of catalytic sites not only provide novel perspectives for FAEO catalysis design, but also have extraordinary significance for the catalyst mechanism exploration. We believe that opportunities and challenges coexist. Through this review, we hope to attract more researchers to jointly promote the progress of FAOR technology in the future.

Acknowledgements

The authors thank the National Natural Science Foundation of China (No. 21905267,), the National Key R&D Program of China (No. 2018YFB1502400), the Strategic Priority Research Program of the Chinese Academy of Sciences (No. XDA21090400), the Department of Science and Technology of Shandong province (No. 2019JZZY010905), and the Jilin Province Science and Technology Development Program (Nos. 20190201300JC, 20170520150JH, and 20200201001JC) for financial support.

References

[1] Haines, A.; Scheelbeek, P.; Abbasi, K. Challenges for health in the Anthropocene epoch. *BMJ* **2019**, *364*, l460.

[2] Logan, B. E.; Rossi, R.; Baek, G.; Shi, L.; O'Connor, J.; Peng, W. Energy use for electricity generation requires an assessment more directly relevant to climate change. *ACS Energy Lett.* **2020**, *5*, 3514–3517.

[3] *Fifth Assessment Report (AR5) Synthesis Report: Climate Change 2014 IPCC* [Online]. Geneva, Switzerland, 2015; pp 151. https://www.ipcc.ch/report/ar5/syr/ (accessed Apr 25, 2021).

[4] Ajdari, F. B.; Kowsari, E.; Shahrak, M. N.; Ehsani, A.; Kiaei, Z.; Torkzaban, H.; Ershadi, M.; Eshkalak, S. K.; Haddadi-Asl, V.; Chinnappan, A. et al. A review on the field patents and recent developments over the application of metal organic frameworks (MOFs) in supercapacitors. *Coord. Chem. Rev.* **2020**, *422*, 213441.

[5] Eltoumi, F. M.; Becherif, M.; Djerdir, A.; Ramadan, H. S. The key issues of electric vehicle charging via hybrid power sources: Techno-economic viability, analysis, and recommendations. *Renew. Sustain. Energy Rev.* **2021**, *138*, 110534.

[6] Jena, P. Clusters and nanomaterials for sustainable energy. *ACS Energy Lett.* **2020**, *5*, 428–429.

[7] Tang, J. Y.; Su, C.; Zhong, Y. J.; Shao, Z. P. Oxide-based precious metal-free electrocatalysts for anion exchange membrane fuel cells: From material design to cell applications. *J. Mater. Chem. A* **2021**, *9*, 3151–3179.

[8] Yun, S. N.; Zhang, Y. W.; Xu, Q.; Liu, J. M.; Qin, Y. Recent advance in new-generation integrated devices for energy harvesting and storage. *Nano Energy* **2019**, *60*, 600–619.

[9] Lei, Z. H.; Lee, J. M.; Singh, G.; Sathish, C. I.; Chu, X. Z.; Al-

Muhtaseb, A. H.; Vinu, A.; Yi, J. B. Recent advances of layered-transition metal oxides for energy-related applications. *Energy Storage Mater.* **2021**, *36*, 514–550.

[10] *International Energy Outlook 2019; U. S. Energy Information Administration* [Online]. https://www.eia.gov/outlooks/archive/ieo19/ (accessed Apr 25, 2021).

[11] *International Energy Outlook 2020; U. S. Energy Information Administration* [Online]. https://www.eia.gov/outlooks/archive/ieo20/ (accessed Apr 25, 2021).

[12] Cao, L. N.; Liu, W.; Luo, Q. Q.; Yin, R. T.; Wang, B.; Weissenrieder, J.; Soldemo, M.; Yan, H.; Lin, Y.; Sun, Z. H. et al. Atomically dispersed iron hydroxide anchored on Pt for preferential oxidation of CO in H_2. *Nature* **2019**, *565*, 631–635.

[13] Durst, J.; Siebel, A.; Simon, C.; Hasché, F.; Herranz, J.; Gasteiger, H. A. New insights into the electrochemical hydrogen oxidation and evolution reaction mechanism. *Energy Environ. Sci.* **2014**, *7*, 2255–2260.

[14] Haider, R.; Wen, Y. C.; Ma, Z. F.; Wilkinson, D. P.; Zhang, L.; Yuan, X. X.; Song, S. Q.; Zhang, J. J. High temperature proton exchange membrane fuel cells: Progress in advanced materials and key technologies. *Chem. Soc. Rev.* **2021**, *50*, 1138–1187.

[15] He, Y. H.; Liu, S. W.; Priest, C.; Shi, Q. R.; Wu, G. Atomically dispersed metal-nitrogen-carbon catalysts for fuel cells: Advances in catalyst design, electrode performance, and durability improvement. *Chem. Soc. Rev.* **2020**, *49*, 3484–3524.

[16] Liu, X.; Zhang, J. F.; Zheng, C. Y.; Xue, J. D.; Huang, T.; Yin, Y.; Qin, Y. Z.; Jiao, K.; Du, Q.; Guiver, M. D. Oriented proton-conductive nano-sponge-facilitated polymer electrolyte membranes. *Energy Environ. Sci.* **2020**, *13*, 297–309.

[17] Shao, M. H.; Chang, Q. W.; Dodelet, J. P.; Chenitz, R. Recent advances in electrocatalysts for oxygen reduction reaction. *Chem. Rev.* **2016**, *116*, 3594–3657.

[18] Zhang, N.; Zhou, T. P.; Chen, M. L.; Feng, H.; Yuan, R. L.; Zhong, C. A.; Yan, W. S.; Tian, Y. C.; Wu, X. J.; Chu W. S. et al. High-purity pyrrole-type FeN_4 sites as a superior oxygen reduction electrocatalyst. *Energy Environ. Sci.* **2020**, *13*, 111–118.

[19] Winter, M.; Brodd, R. J. What are batteries, fuel cells, and supercapacitors? *Chem. Rev.* **2004**, *104*, 4245–4270.

[20] Zhang, J. W.; Chen, M. S.; Li, H. Q.; Li, Y. J.; Ye, J. Y.; Cao, Z. M.; Fang, M. L.; Kuang, Q.; Zheng, J.; Xie, Z. X. Stable palladium hydride as a superior anode electrocatalyst for direct formic acid fuel cells. *Nano Energy* **2018**, *44*, 127–134.

[21] Ye, L.; Mahadi, A. H.; Saengruengrit, C.; Qu, J.; Xu, F.; Fairclough, S. M.; Young, N.; Ho, P. L.; Shan, J. J.; Nguyen, L. et al. Ceria nanocrystals supporting Pd for formic acid electrocatalytic oxidation: Prominent polar surface metal support interactions. *ACS Catal.* **2019**, *9*, 5171–5177.

[22] Yang, L.; Li, G. Q.; Chang, J. F.; Ge, J. J.; Liu, C. P.; Vladimir, F.; Wang, G. L.; Jin, Z.; Xing, W. Sea urchin-like $Au_{core}@Pd_{shell}$ electrocatalysts with high FAOR performance: Coefficient of lattice strain and electrochemical surface area. *Appl. Catal. B:Environ.* **2020**, *260*, 118200.

[23] Wang, X.; Meng, Q. L.; Gao, L. Q.; Jin, Z.; Ge, J. J.; Liu, C. P.; Xing, W. Recent progress in hydrogen production from formic acid decomposition. *Int. J. Hydrogen Energy* **2018**, *43*, 7055–7071.

[24] Wang, F. L.; Xue, H. G.; Tian, Z. Q.; Xing, W.; Feng, L. G. Fe_2P as a novel efficient catalyst promoter in Pd/C system for formic acid electro-oxidation in fuel cells reaction. *J. Power Sources* **2018**, *375*, 37–42.

[25] Gao, N. X.; Ma, R. P.; Wang, X.; Jin, Z.; Hou, S.; Xu, W. L.; Meng, Q. L.; Ge, J. J.; Liu, C. P.; Xing, W. Activating the Pd-Based catalysts via tailoring reaction interface towards formic acid dehydrogenation. *Int. J. Hydrogen Energy* **2020**, *45*, 17575–17582.

[26] Dong, Q. Z.; Wu, M. M.; Mei, D. H.; Shao, Y. Y.; Wang, Y.; Liu, J.; Li, H. Z.; Hong, L. Y. Multifunctional Pd-Sn electrocatalysts enabled by *in situ* formed SnO_x and TiC triple junctions. *Nano Energy* **2018**, *53*, 940–948.

[27] Schill, W. P. Electricity storage and the renewable energy transition. *Joule* **2020**, *4*, 2059–2064.

[28] Liu, P. X. ; Qiao, J. L. A high-performance continuous flow MEA reactor for electroreduction CO_2 to formate. In *ECS Meeting Abstracts*, 2021, pp 1168.

[29] Gao, Z. Q. ; Li, J. J. ; Zhang, Z. C. ; Hu, W. P. Recent advances in carbon-based materials for electrochemical CO_2 reduction reaction. *Chin. Chem. Lett.*, in press, https://doi.org/10.1016/j.cclet.2021.09.037.

[30] Fukuzumi, S. Production of liquid solar fuels and their use in fuel cells. *Joule* **2017**, *1*, 689–738.

[31] Eppinger, J.; Huang, K. W. Formic acid as a hydrogen energy carrier. *ACS Energy Lett.* **2017**, *2*, 188–195.

[32] Chatterjee, S.; Dutta, I.; Lum, Y.; Lai, Z. P.; Huang, K. W. Enabling storage and utilization of low-carbon electricity: Power to formic acid. *Energy Environ. Sci.* **2021**, *14*, 1194–1246.

[33] Arai, T.; Sato, S.; Kajino, T.; Morikawa, T. Solar CO_2 reduction using H_2O by a semiconductor/metal-complex hybrid photocatalyst: Enhanced efficiency and demonstration of a wireless system using $SrTiO_3$ photoanodes. *Energy Environ. Sci.* **2013**, *6*, 1274–1282.

[34] Parsons, R.; VanderNoot, T. The oxidation of small organic molecules: A survey of recent fuel cell related research. *J. Electroanal. Chem. Interfacial Electrochem.* **1988**, *257*, 9–45.

[35] Marković, N. M.; Ross, P. Jr. Surface science studies of model fuel cell electrocatalysts. *Surf. Sci. Rep.* **2002**, *45*, 117–229.

[36] Fang, Z. Y.; Chen, W. Recent advances in formic acid electro-oxidation: From the fundamental mechanism to electrocatalysts. *Nanoscale Adv.* **2021**, *3*, 94–105.

[37] Müller, E. Zur elektrolytischen Oxydation der Ameisensäure. *Zeitsch. Elektr. Angew. Phys. Chem.* **1927**, *33*, 561–568.

[38] Müller, E. Die elektrolytische Oxydation der Ameisensäure. *Zeitsch. Elektr. Angew. Phys. Chem.* **1923**, *29*, 264–274.

[39] Mülle, E.; Tanaka, S. Über die pulsierende elektrolytische Oxydation der Ameisensäure. *Zeitsch. Elektr. Angew. Phys. Chem.* **1928**, *34*, 256–264.

[40] Herasymenko, P. Adsorption processes in anodic oxidation of formic acid. *Ukr. Khim. Zh.* **1929**, *4*, 439–452.

[41] Schwabe, K. Über Potentialmessungen an Metallkatalysatoren in wäßriger Lösung. *Z. Elektr. , Berichte Bunseng. Phys. Chem.* **1957**, *61*, 744–752.

[42] Buck, R. P.; Griffith, L. R. Voltammetric and chronopotentiometric study of the anodic oxidation of methanol, formaldehyde, and formic acid. *J. Electrochem. Soc.* **1962**, *109*, 1005.

[43] Slott, R. Electrochemical oxidation of formic acid; Massachusetts Inst of Tech Cambridge: 1963.

[44] Rhodes, D. R.; Steigelmann, E. F. Catalytic decomposition of aqueous formic acid on platinum electrodes. *J. Electrochem. Soc.* **1965**, *112*, 16.

[45] Conway, B. E.; Dzieciuch, M. New approaches to the study of electrochemical decarboxylation and the Kolbe reaction: Part I. The model reaction with formate. *Canadian J. Chem.* **1963**, *41*, 21–37.

[46] Giner, J. The anodic oxidation of methanol and formic acid and the reductive. Adsorption of CO_2. *Electrochim. Acta* **1964**, *9*, 63–77.

[47] Breiter, M. W. Anodic oxidation of formic acid on platinum—I. Adsorption of formic acid, oxygen, and hydrogen in perchloric acid solutions. *Electrochim. Acta* **1963**, *8*, 447–456.

[48] Breiter, M. W. Anodic oxidation of formic acid on platinum—II. Interpretation of potentiostatic current/potential curves. Reaction mechanism in perchloric acid solutions. *Electrochim. Acta* **1963**, *8*, 457–470.

[49] Warner, T. B.; Schuldiner, S. Effects of oxygen absorbed in the skin of a platinum electrode on the determination of carbon monoxide adsorption. *J. Phys. Chem.* **1965**, *69*, 4048–4049.

[50] Brummer, S. B.; Makrides, A. C. Adsorption and oxidation of formic acid on smooth platinum electrodes in perchloric acid solutions. *J. Phys. Chem.* **1964**, *68*, 1448–1459.

[51] Brummer, S. B.; Ford, J. I. Galvanostatic studies of carbon monoxide adsorption on platinum electrodes. *J. Phys. Chem.* **1965**, *69*, 1355–1362.

[52] Brummer, S. B. The use of large anodic galvanostatic transients to evaluate the maximum adsorption on platinum from formic acid solutions. *J. Phys. Chem.* **1965**, *69*, 562–571.

[53] Brummer, S. B. The correction for electrode oxidation in the estimation of adsorbed CO on smooth platinum by anodic stripping.

J. Phys. Chem. **1965**, *69*, 4049–4050.
[54] Breiter, M. W. Comparative oxidation of chemisorbed carbon monoxide, reduced carbon dioxide and species formed during the methanol oxidation. *J. Electroanal. Chem. Interfacial Electrochem.* **1968**, *19*, 131–136.
[55] Breiter, M. W. Nature of strongly adsorbed species formed on platinizedplatinum after the addition of methanol, formic acid, and formaldehyde. *J. Electroanal. Chem. Interfacial Electrochem.* **1967**, *15*, 221–226.
[56] Taylor, A. H.; Pearce, R. D.; Brummer, S. B. Effect of adsorbed layers on the anodic oxidation of simple organic compounds. Part 2. —Role of adsorbed HCOOH species. *Trans. Faraday Soc.* **1971**, *67*, 801–808.
[57] Taylor, A. H.; Pearce, R. D.; Brummer, S. B. Effect of adsorbed layers on the anodic oxidation of simple organic compounds. Part 1. —Time variations during the oxidation of HCOOH and effect of added Cl^-. *Trans. Faraday Soc.* **1970**, *66*, 2076–2084.
[58] Capon, A.; Parsons, R. The oxidation of formic acid at noble metal electrodes Part III. Intermediates and mechanism on platinum electrodes. *J. Electroanal. Chem. Interfacial Electrochem.* **1973**, *45*, 205–231.
[59] Capon, A.; Parsons, R. The oxidation of formic acid on noble metal electrodes: II. A comparison of the behaviour of pure electrodes. *J. Electroanal. Chem. Interfacial Electrochem.* **1973**, *44*, 239–254.
[60] Capon, A.; Parson, R. The oxidation of formic acid at noble metal electrodes: I. Review of previous work. *J. Electroanal. Chem. Interfacial Electrochem.* **1973**, *44*, 1–7.
[61] Yeager, E. Non-traditional approaches to the study of solid-electrolyte interfaces: Problem overview. *Surf. Sci.* **1980**, *101*, 1–22.
[62] Kuwana, T. Optically coupled electrochemical studies. *Berichte Bunseng. Phys. Chem.* **1973**, *77*, 858–871.
[63] Jeanmaire, D. L.; Van Duyne, R. P. Resonance Raman spectroelectrochemistry. 3. Tunable dye laser excitation spectroscopy of the lowest 2B1u excited state of the tetracyanoquinodimethane anion radical. *J. Am. Chem. Soc.* **1976**, *98*, 4034–4039.
[64] Fleischmann, M.; Hendra, P. J.; McQuillan, A. J. Raman spectra from electrode surfaces. *J. Chem. Soc. , Chem. Commun.* **1973**, *3*, 80–81.
[65] Cooney, R. P.; Fleischmann, M.; Hendra, P. J. Raman spectrum of carbon monoxide on a platinum electrode surface. *J. Chem. Soc. , Chem. Commun.* **1977**, 235–237.
[66] Bewick, A.; Kunimatsu, K. Infra red spectroscopy of the electrode-electrolyte interphase. *Surf. Sci.* **1980**, *101*, 131–138.
[67] Bewick, A.; Kunimatsu, K.; Pons, B. S. Infra red spectroscopy of the electrode-electrolyte interphase. *Electrochim. Acta* **1980**, *25*, 465–468.
[68] Bewick, A.; Kunimatsu, K.; Robinson, J.; Russell, J. W. IR vibrational spectroscopy of species in the electrode-electrolyte solution interphase. *J. Electroanal. Chem. Interfacial Electrochem.* **1981**, *119*, 175–185.
[69] Bewick, A.; Kunimatsu, K.; Pons, B. S.; Russell, J. W. Electrochemically modulated infrared spectroscopy (EMIRS): Experimental details. *J. Electroanal. Chem. Interfacial Electrochem.* **1984**, *160*, 47–61.
[70] Beden, B.; Lamy, C.; Bewick, A.; Kunimatsu, K. Electrosorption of methanol on a platinum electrode. IR spectroscopic evidence for adsorbed CO species. *J. Electroanal. Chem. Interfacial Electrochem.* **1981**, *121*, 343–347.
[71] Beden, B.; Bewick, A.; Lamy, C. A comparative study of formic acid adsorption on a platinum electrode by both electrochemical and emirs techniques. *J. Electroanal. Chem. Interfacial Electrochem.* **1983**, *150*, 505–511.
[72] Beden, B.; Bewick, A.; Lamy, C. A study by electrochemically modulated infrared reflectance spectroscopy of the electrosorption of formic acid at a platinum electrode. *J. Electroanal. Chem. Interfacial Electrochem.* **1983**, *148*, 147–160.
[73] Sun, S. G.; Clavilier, J.; Bewick, A. The mechanism of electrocatalytic oxidation of formic acid on Pt (100) and Pt (111) in sulphuric acid solution: An emirs study. *J. Electroanal. Chem. Interfacial Electrochem.* **1988**, *240*, 147–159.
[74] Juanto, S.; Beden, B.; Hahn, F.; Leger, J. M.; Lamy, C. Infrared spectroscopic study of the methanol adsorbates at a platinum electrode: Part II. The Pt (100) surface in an acid medium. *J. Electroanal. Chem. Interfacial Electrochem.* **1987**, *237*, 119–129.
[75] Beden, B.; Hahn, F.; Juanto, S.; Lamy, C.; Leger, J. M. Infrared spectroscopic study of the methanol adsorbates at a platinum electrode: Part I. Influence of the bulk concentration of methanol upon the nature of the adsorbates. *J. Electroanal. Chem. Interfacial Electrochem.* **1987**, *225*, 215–225.
[76] Kunimatsu, K.; Kita, H. Infrared spectroscopic study of methanol and formic acid absorbates on a platinum electrode: Part II. Role of the linear CO(a) derived from methanol and formic acid in the electrocatalytic oxidation of CH_3OH and HCOOH. *J. Electroanal. Chem. Interfacial Electrochem.* **1987**, *218*, 155–172.
[77] Corrigan, D. S.; Weaver, M. J. Mechanisms of formic acid, methanol, and carbon monoxide electrooxidation at platinum as examined by single potential alteration infrared spectroscopy. *J. Electroanal. Chem. Interfacial Electrochem.* **1988**, *241*, 143–162.
[78] Corrigan, D. S.; Leung, L. W. H.; Weaver, M. J. Single potential-alteration surface infrared spectroscopy: Examination of absorbed species involved in irreversible electrode reactions. *Anal. Chem.* **1987**, *59*, 2252–2256.
[79] Chang, S. C.; Leung, L. W. H.; Weaver, M. J. Metal crystallinity effects in electrocatalysis as probed by real-time FTIR spectroscopy: Electrooxidation of formic acid, methanol, and ethanol on ordered low-index platinum surfaces. *J. Phys. Chem.* **1990**, *94*, 6013–6021.
[80] Bruckenstein, S.; Gadde, R. R. Use of a porous electrode for *in situ* mass spectrometric determination of volatile electrode reaction products. *J. Am. Chem. Soc.* **1971**, *93*, 793–794.
[81] Wolter, O.; Heitbaum, J. The adsorption of CO on a porous Pt-electrode in sulfuric acid studied by DEMS. *Ber. Bunseng. Phys. Chem.* **1984**, *88*, 6–10.
[82] Wolter, O.; Heitbaum, J. Differential electrochemical mass spectroscopy (DEMS)—A new method for the study of electrode processes. *Ber. Bunseng. Phys. Chem.* **1984**, *88*, 2–6.
[83] Wolter, O.; Willsau, J.; Heitbaum, J. Reaction pathways of the anodic oxidation of formic acid on Pt evidenced by ^{18}O labeling—A DEMS study. *J. Electrochem. Soc.* **1985**, *132*, 1635–1638.
[84] Willsau, J.; Heitbaum, J. Analysis of adsorbed intermediates and determination of surface potential shifts by dems. *Electrochim. Acta* **1986**, *31*, 943–948.
[85] Willsau, J.; Heitbaum, J. Mass spectroscopic detection of the hydrogen in methanol-adsorbate. *J. Electroanal. Chem. Interfacial Electrochem.* **1985**, *185*, 181–183.
[86] Jeanmaire, D. L.; Van Duyne, R. P. Surface Raman spectroelectrochemistry: Part I. Heterocyclic, aromatic, and aliphatic amines adsorbed on the anodized silver electrode. *J. Electroanal. Chem. Interfacial Electrochem.* **1977**, *84*, 1–20.
[87] Chang, R. K.; Laube, B. L. Surface-enhanced Raman scattering and nonlinear optics applied to electrochemistry. *Crit. Rev. Solid State Mater. Sci.* **1984**, *12*, 1–73.
[88] Albrecht, M. G.; Creighton, J. A. Anomalously intense Raman spectra of pyridine at a silver electrode. *J. Am. Chem. Soc.* **1977**, *99*, 5215–5217.
[89] Zhang, Y.; Weaver, M. J. Application of surface-enhanced Raman spectroscopy to organic electrocatalytic systems: Decomposition and electrooxidation of methanol and formic acid on gold and platinum-film electrodes. *Langmuir* **1993**, *9*, 1397–1403.
[90] Leung, L. W. H.; Weaver, M. J. Extending surface-enhanced Raman spectroscopy to transition-metal surfaces: Carbon monoxide adsorption and electrooxidation on platinum-and palladium-coated gold electrodes. *J. Am. Chem. Soc.* **1987**, *109*, 5113–5119.
[91] Weaver, M. J.; Corrigan, D. S.; Gao, P.; Gosztola, D.; Leung, L. W. H. Some applications of surface Raman and infrared spectroscopies to mechanistic electrochemistry involving adsorbed species. *J. Electron Spectros. Relat. Phenomena* **1987**, *45*, 291–302.
[92] Tian, Z. Q.; Ren, B.; Wu, D. Y. Surface-enhanced Raman

scattering: From noble to transition metals and from rough surfaces to ordered nanostructures. *J. Phys. Chem. B* **2002**, *106*, 9463–9483.
[93] Cao, P. G.; Zhong, Q. L.; Sun, Y. H.; Gu, R. A. Dissociation and electrooxidation of formic acid at platinum in nonaqueous solutions as probed by *in situ* surface-enhanced Raman spectroscopy. *Chem. Phys. Lett.* **2003**, *376*, 806–811.
[94] Samjeské, G.; Miki, A.; Ye, S.; Osawa, M. Mechanistic study of electrocatalytic oxidation of formic acid at platinum in acidic solution by time-resolved surface-enhanced infrared absorption spectroscopy. *J. Phys. Chem. B* **2006**, *110*, 16559–16566.
[95] Samjeské, G.; Osawa, M. Current oscillations during formic acid oxidation on a Pt electrode: Insight into the mechanism by time-resolved IR spectroscopy. *Angew. Chem. , Int. Ed.* **2005**, *44*, 5694–5698.
[96] Chen, Y. X.; Heinen, M.; Jusys, Z.; Behm, R. J. Kinetics and mechanism of the electrooxidation of formic acid—Spectroelectrochemical studies in a flow cell. *Angew. Chem., Int. Ed.* **2006**, *45*, 981–985.
[97] Chen, Y. X.; Heinen, M.; Jusys, Z.; Behm, R. J. Bridge-bonded formate: Active intermediate or spectator species in formic acid oxidation on a Pt film electrode. *Langmuir* **2006**, *22*, 10399–10408.
[98] Neurock, M.; Janik, M.; Wieckowski, A. A first principles comparison of the mechanism and site requirements for the electrocatalytic oxidation of methanol and formic acid over Pt. *Faraday Discuss.* **2009**, *140*, 363–378.
[99] Wang, H. F.; Liu, Z. P. Formic acid oxidation at Pt/H_2O interface from periodic DFT calculations integrated with a continuum solvation model. *J. Phys. Chem. C* **2009**, *113*, 17502–17508.
[100] Gao, W.; Mueller, J. E.; Jiang, Q.; Jacob, T. The role of Co-adsorbed CO and OH in the electrooxidation of formic acid on Pt(111). *Angew. Chem. , Int. Ed.* **2012**, *51*, 9448–9452.
[101] Gao, W.; Keith, J. A.; Anton, J.; Jacob, T. Theoretical elucidation of the competitive electro-oxidation mechanisms of formic acid on Pt (111). *J. Am. Chem. Soc.* **2010**, *132*, 18377–18385.
[102] Gao, W.; Keith, J. A.; Anton, J.; Jacob, T. Oxidation of formic acid on the Pt(111) surface in the gas phase. *Dalton Trans.* **2010**, *39*, 8450–8456.
[103] Joo, J.; Uchida, T.; Cuesta, A.; Koper, M. T.; Osawa, M. Importance of acid-base equilibrium in electrocatalytic oxidation of formic acid on platinum. *J. Am. Chem. Soc.* **2013**, *135*, 9991–9994.
[104] Ferre-Vilaplana, A.; Perales-Rondón, J. V.; Buso-Rogero, C.; Feliu, J. M.; Herrero, E. Formic acid oxidation on platinum electrodes: A detailed mechanism supported by experiments and calculations on well-defined surfaces. *J. Mater. Chem. A* **2017**, *5*, 21773–21784.
[105] Zhu, X. W.; Huang, J. Modeling electrocatalytic oxidation of formic acid at platinum. *J. Electrochem. Soc.* **2020**, *167*, 013515.
[106] Zhang, M. K.; Chen, W.; Wei, Z.; Xu, M. L.; He, Z. D.; Cai, J.; Chen, Y. X.; Santos, E. Mechanistic implication of the pH effect and H/D kinetic isotope effect on $HCOOH/HCOO^-$ oxidation at Pt electrodes: A study by computer simulation. *ACS Catal.* **2021**, *11*, 6920–6930.
[107] Feng, L. G.; Chang, J. F.; Jiang, K.; Xue, H. G.; Liu, C. P.; Cai, W. B.; Xing, W.; Zhang, J. J. Nanostructured palladium catalyst poisoning depressed by cobalt phosphide in the electro-oxidation of formic acid for fuel cells. *Nano Energy* **2016**, *30*, 355–361.
[108] Wang, S. L.; Chang, J. F.; Xue, H. G.; Xing, W.; Feng, L. G. Catalytic stability study of a $Pd\text{-}Ni_2P/C$ catalyst for formic acid electrooxidation. *ChemElectroChem* **2017**, *4*, 1243–1249.
[109] Shi, Y. F.; Schimmenti, R.; Zhu, S. Q.; Venkatraman, K.; Chen, R. H.; Chi, M. F.; Shao, M. H.; Mavrikakis, M.; Xia, Y. N. Solution-phase synthesis of $PdH_{0.706}$ nanocubes with enhanced stability and activity toward formic acid oxidation. *J. Am. Chem. Soc.* **2022**, *144*, 2556–2568.
[110] Yu, N. F.; Tian, N.; Zhou, Z. Y.; Sheng, T.; Lin, W. F.; Ye, J. Y.; Liu, S.; Ma, H. B.; Sun, S. G. Pd nanocrystals with continuously tunable high-index facets as a model nanocatalyst. *ACS Catal.* **2019**, *9*, 3144–3152.
[111] Sun, S. G.; Yang, Y. Y. Studies of kinetics of HCOOH oxidation on Pt(100), Pt(110), Pt(111), Pt(510) and Pt(911) single crystal electrodes. *J. Electroanal. Chem.* **1999**, *467*, 121–131.
[112] Hoshi, N.; Kida, K.; Nakamura, M.; Nakada, M.; Osada, K. Structural effects of electrochemical oxidation of formic acid on single crystal electrodes of palladium. *J. Phys. Chem. B* **2006**, *110*, 12480–12484.
[113] Elnabawy, A. O.; Herron, J. A.; Scaranto, J.; Mavrikakis, M. Structure sensitivity of formic acid electrooxidation on transition metal surfaces: A first-principles study. *J. Electrochem. Soc.* **2018**, *165*, J3109.
[114] Choi, S. I.; Herron, J. A.; Scaranto, J.; Huang, H.; Wang, Y.; Xia, X. H.; Lv, T.; Park, J.; Peng, H. C.; Mavrikakis, M. et al. A comprehensive study of formic acid oxidation on palladium nanocrystals with different types of facets and twin defects. *ChemCatChem* **2015**, *7*, 2077–2084.
[115] Iwasita, T.; Nart, F. C.; Lopez, B.; Vielstich, W. On the study of adsorbed species at platinum from methanol, formic acid and reduced carbon dioxide via *in situ* FT-*ir* spectroscopy. *Electrochim. Acta* **1992**, *37*, 2361–2367.
[116] Zhou, Y.; Liu, D. Y.; Liu, Z.; Feng, L. G.; Yang, J. Interfacial Pd-O-Ce linkage enhancement boosting formic acid electrooxidation. *ACS Appl. Mater. Interfaces* **2020**, *12*, 47065–47075.
[117] Bao, Y. F.; Zha, M.; Sun, P. L.; Hu, G. Z.; Feng, L. G. PdNi/N-doped graphene aerogel with over wide potential activity for formic acid electrooxidation. *J. Energy Chem.* **2021**, *59*, 748–754.
[118] Bao, Y. F.; Feng, L. G. Formic acid electro-oxidation catalyzed by PdNi/graphene aerogel. *Acta Phys. -Chim. Sin.* **2021**, *37*, 2008031.
[119] Leiva, E.; Iwasita, T.; Herrero, E.; Feliu, J. M. Effect of adatoms in the electrocatalysis of HCOOH oxidation. A theoretical model. *Langmuir* **1997**, *13*, 6287–6293.
[120] Zhou, Y.; Liu, D. Y.; Qiao, W.; Liu, Z.; Yang, J.; Feng, L. G. Ternary synergistic catalyst system of $Pt\text{-}Cu\text{-}Mo_2C$ with high activity and durability for alcohol oxidation. *Mater. Today Phys.* **2021**, *17*, 100357.
[121] Marković, N. M.; Gasteiger, H. A.; Ross, P. N. Jr.; Jiang, X. D.; Villegas, I.; Weaver, M. J. Electro-oxidation mechanisms of methanol and formic acid on Pt-Ru alloy surfaces. *Electrochim. Acta* **1995**, *40*, 91–98.
[122] Kizhakevariam, N.; Weaver, M. J. Structure and reactivity of bimetallic electrochemical interfaces: Infrared spectroscopic studies of carbon monoxide adsorption and formic acid electrooxidation on antimony-modified Pt(100) and Pt(111). *Surf. Sci.* **1994**, *310*, 183–197.
[123] Gasteiger, H. A.; Marković, N.; Ross, P. N. Jr.; Cairns, E. J. Electro-oxidation of small organic molecules on well-characterized Pt-Ru alloys. *Electrochim. Acta* **1994**, *39*, 1825–1832.
[124] Fang, B.; Feng, L. G. PtCo-NC catalyst derived from the pyrolysis of Pt-incorporated ZIF-67 for alcohols fuel electrooxidation. *Acta Phys. -Chim. Sin.* **2020**, *36*, 1905023.
[125] Chang, S. C.; Ho, Y.; Weaver, M. J. Applications of real-time infrared spectroscopy to electrocatalysis at bimetallic surfaces: I. Electrooxidation of formic acid and methanol on bismuth-modified Pt(111) and Pt(100). *Surf. Sci.* **1992**, *265*, 81–94.
[126] Bittins-Cattaneo, B.; Iwasita, T. Electrocatalysis of methanol oxidation by adsorbed tin on platinum. *J. Electroanal. Chem. Interfacial Electrochem.* **1987**, *238*, 151–161.
[127] Angerstein-Kozlowska, H.; MacDougall, B.; Conway, B. E. Origin of activation effects of acetonitrile and mercury in electrocatalytic oxidation of formic acid. *J. Electrochem. Soc.* **1973**, *120*, 756–766.
[128] Vidal-Iglesias, F.; Solla-Gullon, J.; Herrero, E.; Aldaz, A.; Feliu, J. Formic acid oxidation on Pd-modified Pt (100) and Pt (111) electrodes: A DEMS study. *Journal of applied electrochemistry* **2006**, *36*, 1207–1214.
[129] Shen, T.; Chen, S. J.; Zeng, R.; Gong, M. M.; Zhao, T. H.; Lu, Y.; Liu, X. P.; Xiao, D. D.; Yang, Y.; Hu, J. P. et al. Tailoring the antipoisoning performance of Pd for formic acid electrooxidation via an ordered PdBi intermetallic. *ACS Catal.* **2020**, *10*, 9977–9985.
[130] Wang, Y. H.; Liang, M. M.; Zhang, Y. J.; Chen, S.; Radjenovic, P.; Zhang, H.; Yang, Z. L.; Zhou, X. S.; Tian, Z. Q.; Li, J. F. Probing interfacial electronic and catalytic properties on well-defined surfaces by using *in situ* Raman spectroscopy. *Angew. Chem.* **2018**, *130*, 11427–11431.
[131] Xie, W. C.; Ling, Y.; Zhang, Y. Z.; Pan, H.; Liu, G. K.; Tang, J. *In-*

situ electrochemical surface-enhanced Raman spectroscopy study of formic acid electrooxidation at variable temperatures by high-frequency heating technology. *Electrochim. Acta* **2018**, *281*, 323–328.

[132] Wasmus, S.; Küver, A. Methanol oxidation and direct methanol fuel cells: A selective review. *J. Electroanal. Chem.* **1999**, *461*, 14–31.

[133] Chen, W.; Yu, A.; Sun, Z. J.; Zhu, B. Q.; Cai, J.; Chen, Y. X. Probing complex eletrocatalytic reactions using electrochemical infrared spectroscopy. *Curr. Opin. Electrochem.* **2019**, *14*, 113–123.

[134] Zhang, X. G.; Arikawa, T.; Murakami, Y.; Yahikozawa, K.; Takasu, Y. Electrocatalytic oxidation of formic acid on ultrafine palladium particles supported on a glassy carbon. *Electrochim. Acta* **1995**, *40*, 1889–1897.

[135] Yang, Y.; Xiong, Y.; Zeng, R.; Lu, X. Y.; Krumov, M.; Huang, X.; Xu, W. X.; Wang, H. S.; DiSalvo, F. J.; Brock, J. D. et al. *Operando* methods in electrocatalysis. *ACS Catal.* **2021**, *11*, 1136–1178.

[136] Pishgar, S.; Gulati, S.; Strain, J. M.; Liang, Y.; Mulvehill, M. C.; Spurgeon, J. M. *In situ* analytical techniques for the investigation of material stability and interface dynamics in electrocatalytic and photoelectrochemical applications. *Small Meth.* **2021**, *5*, 2100322.

[137] Li, W. X.; Sun, J. H.; Gao, Y. X.; Zhang, Y.; Ouyang, J.; Na, N. Monitoring of electrochemical reactions on different electrode configurations by ambient mass spectrometry. *TrAC Trends Anal. Chem.* **2021**, *135*, 116180.

[138] Anastasijevic, N. A.; Baltruschat, H.; Heitbaum, J. DEMS as a tool for the investigation of dynamic processes: Galvanostatic formic acid oxidation on a Pt electrode. *J. Electroanal. Chem. Interfacial Electrochem.* **1989**, *272*, 89–100.

[139] Xu, Z. Z.; Liang, Z. B.; Guo, W. H.; Zou, R. Q. *In situ*/*operando* vibrational spectroscopy for the investigation of advanced nanostructured electrocatalysts. *Coord. Chem. Rev.* **2021**, *436*, 213824.

[140] Ikegaya, S.; Motobayashi, K.; Ikeda, K. Long-range surface plasmon enhanced Raman spectroscopy at highly damping platinum electrodes. *J. Raman Spectrosc.* **2021**, *52*, 420–430.

[141] Muralidharan, R.; McIntosh, M.; Li, X. *In situ* surface-enhanced Raman spectroscopic study of formic acid electrooxidation on spontaneously deposited platinum on gold. *Phys. Chem. Chem. Phy.* **2013**, *15*, 9716–9725.

[142] Li, J. F.; Huang, Y. F.; Ding, Y.; Yang, Z. L.; Li, S. B.; Zhou, X. S.; Fan, F. R.; Zhang, W.; Zhou, Z. Y.; Wu, D. Y. et al. Shell-isolated nanoparticle-enhanced Raman spectroscopy. *Nature* **2010**, *464*, 392–395.

[143] Wu, D. Y.; Li, J. F.; Ren, B.; Tian, Z. Q. Electrochemical surface-enhanced Raman spectroscopy of nanostructures. *Chem. Soc. Rev.* **2008**, *37*, 1025–1041.

[144] Janik, M. J.; Taylor, C. D.; Neurock, M. First principles analysis of the electrocatalytic oxidation of methanol and carbon monoxide. *Top. Catal.* **2007**, *46*, 306–319.

[145] Janik, M. J.; Neurock, M. A first principles analysis of the electro-oxidation of CO over Pt(111). *Electrochim. Acta* **2007**, *52*, 5517–5528.

[146] Desai, S.; Neurock, M. A first principles analysis of CO oxidation over Pt and $Pt_{66.7\%}Ru_{33.3\%}$(111) surfaces. *Electrochim. Acta* **2003**, *48*, 3759–3773.

[147] Anderson, A. B.; Neshev, N. M.; Sidik, R. A.; Shiller, P. Mechanism for the electrooxidation of water to OH and O bonded to platinum: Quantum chemical theory. *Electrochim. Acta* **2002**, *47*, 2999–3008.

[148] Anderson, A. B.; Grantscharova, E. Catalytic effect of ruthenium in ruthenium-platinum alloys on the electrooxidation of methanol. Molecular orbital theory. *J. Phys. Chem.* **1995**, *99*, 9149–9154.

[149] Anderson, A. B. O_2 reduction and CO oxidation at the Pt-electrolyte interface. The role of H_2O and OH adsorption bond strengths. *Electrochim. Acta* **2002**, *47*, 3759–3763.

[150] Meng, F. H.; Yang, M.; Li, Z. Q.; Zhang, R. G. HCOOH dissociation over the Pd-decorated Cu bimetallic catalyst: The role of the Pd ensemble in determining the selectivity and activity. *Appl. Surf. Sci.* **2020**, *511*, 145554.

[151] Yang, L.; Wang, X.; Liu, D. P.; Cui, G. M.; Dou, B. L.; Wang, J. Efficient anchoring of nanoscale Pd on three-dimensional carbon hybrid as highly active and stable catalyst for electro-oxidation of formic acid. *Appl. Catal. B:Environ.* **2020**, *263*, 118304.

[152] Xu, Y.; Wang, M. Z.; Yu, S. S.; Ren, T. L.; Ren, K. L.; Wang, Z. Q.; Li, X. N.; Wang, L.; Wang, H. J. Electronic structure control over Pd nanorods by B, P-co-doping enables enhanced electrocatalytic performance. *Chem. Eng. J.* **2021**, *421*, 127751.

[153] Yang, N. L.; Zhang, Z. C.; Chen, B.; Huang, Y.; Chen, J. Z.; Lai, Z. C.; Chen, Y.; Sindoro, M.; Wang, A. L.; Cheng, H. F. et al. Synthesis of ultrathin PdCu alloy nanosheets used as a highly efficient electrocatalyst for formic acid oxidation. *Adv. Mater.* **2017**, *29*, 1700769.

[154] Tang, M.; Chen, W.; Luo, S. P.; Wu, X. T.; Fan, X. K.; Liao, Y. J.; Song, X.; Cheng, Y.; Li, L. X.; Tan, L. et al. Trace Pd modified intermetallic PtBi nanoplates towards efficient formic acid electrocatalysis. *J. Mater. Chem. A* **2021**, *9*, 9602–9608.

[155] Choi, M.; Ahn, C. Y.; Lee, H.; Kim, J. K.; Oh, S. H.; Hwang, W.; Yang, S.; Kim, J.; Kim, O. H.; Choi, I. et al. Bi-modified Pt supported on carbon black as electro-oxidation catalyst for 300 W formic acid fuel cell stack. *Appl. Catal. B:Environ.* **2019**, *253*, 187–195.

[156] Bao, Y. F.; Liu, H.; Liu, Z.; Wang, F. L.; Feng, L. G. Pd/FeP catalyst engineering via thermal annealing for improved formic acid electrochemical oxidation. *Appl. Catal. B:Environ.* **2020**, *274*, 119106.

[157] Li, J. R.; Jilani, S. Z.; Lin, H. H.; Liu, X. M.; Wei, K. C.; Jia, Y. K.; Zhang, P.; Chi, M. F.; Tong, Y. Y. J.; Xi, Z. et al. Ternary CoPtAu nanoparticles as a general catalyst for highly efficient electro-oxidation of liquid fuels. *Angew. Chem. , Int. Ed.* **2019**, *58*, 11527–11533.

[158] Jiang, J. X.; Ding, W.; Li, W.; Wei, Z. D. Freestanding single-atom-layer Pd-based catalysts: Oriented splitting of energy bands for unique stability and activity. *Chem* **2020**, *6*, 431–447.

[159] Luo, S. P.; Chen, W.; Cheng, Y.; Song, X.; Wu, Q. L.; Li, L. X.; Wu, X. T.; Wu, T. H.; Li, M. R.; Yang, Q. et al. Trimetallic synergy in intermetallic PtSnBi nanoplates boosts formic acid oxidation. *Adv. Mater.* **2019**, *31*, 1903683.

[160] Zhang, L. Y.; Wang, F. Q.; Wang, S.; Huang, H. W.; Meng, X. M.; Ouyang, Y. R.; Yuan, W. Y.; Guo, C. X.; Li, C. M. Layered and heterostructured Pd/PdWCr sheet-assembled nanoflowers as highly active and stable electrocatalysts for formic acid oxidation. *Adv. Funct. Mater.* **2020**, *30*, 2003933.

[161] Xie, Y. X.; Dimitrov, N. Ultralow Pt loading nanoporous Au-Cu-Pt thin film as highly active and durable catalyst for formic acid oxidation. *Appl. Catal. B:Environ.* **2020**, *263*, 118366.

[162] Sang, Q. Q.; Yin, S.; Liu, F.; Yin, H. M.; He, J.; Ding, Y. Highly coordinated Pd overlayers on nanoporous gold for efficient formic acid electro-oxidation. *Nano Res.* **2021**, *14*, 3502–3508.

[163] Fan, H. S.; Cheng, M.; Wang, L.; Song, Y. J.; Cui, Y. M.; Wang, R. M. Extraordinary electrocatalytic performance for formic acid oxidation by the synergistic effect of Pt and Au on carbon black. *Nano Energy* **2018**, *48*, 1–9.

[164] Xu, Y.; Yu, S. S.; Ren, T. L.; Li, C. J.; Yin, S. L.; Wang, Z. Q.; Li, X. N.; Wang, L.; Wang, H. J. A quaternary metal-metalloid-nonmetal electrocatalyst: B, P-co-doping into PdRu nanospine assemblies boosts the electrocatalytic capability toward formic acid oxidation. *J. Mater. Chem. A* **2020**, *8*, 2424–2429.

[165] Jiang, T.; Mowbray, D. J.; Dobrin, S.; Falsig, H.; Hvolbæk, B.; Bligaard, T.; Nørskov, J. K. Trends in CO oxidation rates for metal nanoparticles and close-packed, stepped, and kinked surfaces. *J. Phys. Chem. C* **2009**, *113*, 10548–10553.

[166] Hammer, B.; Nielsen, O. H.; Nrskov, J. K. Structure sensitivity in adsorption: CO interaction with stepped and reconstructed Pt surfaces. *Catal. Lett.* **1997**, *46*, 31–35.

[167] Kim, J.; Roh, C. W.; Sahoo, S. K.; Yang, S.; Bae, J.; Han, J. W.; Lee, H. Highly durable platinum single-atom alloy catalyst for electrochemical reactions. *Adv. Energy Mater.* **2018**, *8*, 1701476.

[168] Li, Z.; Chen, Y. J.; Ji, S. F.; Tang, Y.; Chen, W. X.; Li, A.; Zhao, J.; Xiong, Y.; Wu, Y. E.; Gong, Y. et al. Iridium single-atom catalyst on nitrogen-doped carbon for formic acid oxidation synthesized using a general host-guest strategy. *Nat. Chem.* **2020**, *12*, 764–772.

[169] Zhang, S.; Xia, R.; Su, Y. Q.; Zou, Y. C.; Hu, C. Y.; Yin, G. P.; Hensen, E. J. M.; Ma, X. B.; Lin, Y. H. 2D surface induced self-assembly of Pd nanocrystals into nanostrings for enhanced formic acid electrooxidation. *J. Mater. Chem. A* **2020**, *8*, 17128–17135.

[170] Shi, W. J.; Park, A. H.; Xu, S. Y.; Yoo, P. J.; Kwon, Y. U. Continuous and conformal thin TiO_2-coating on carbon support makes Pd nanoparticles highly efficient and durable electrocatalyst. *Appl. Catal. B:Environ.* **2021**, *284*, 119715.

[171] Seselj, N.; Engelbrekt, C.; Ding, Y.; Hjuler, H. A.; Ulstrup, J.; Zhang, J. D. Tailored electron transfer pathways in Au_{core}/Pt_{shell}-graphene nanocatalysts for fuel cells. *Adv. Energy Mater.* **2018**, *8*, 1702609.

[172] Pajić, M. N. K.; Stevanović, S. I.; Radmilović, V. V.; Gavrilović-Wohlmuther, A.; Zabinski, P.; Elezović, N. R.; Radmilović, V. R.; Gojković, S. L.; Jovanović, V. M. Dispersion effect in formic acid oxidation on PtAu/C nanocatalyst prepared by water-in-oil microemulsion method. *Appl. Catal. B:Environ.* **2019**, *243*, 585–593.

[173] El-Nagar, G. A.; Dawood, K. M.; El-Deab, M. S.; Al-Andouli, B. E. Efficient direct formic acid fuel cell (DFAFC) anode of nano-sized palladium complex: High durability and activity origin. *Appl. Catal. B:Environ.* **2017**, *213*, 118–126.

[174] Liang, W. K.; Wang, Y. W.; Zhao, L.; Guo, W.; Li, D.; Qin, W.; Wu, H. H.; Sun, Y. H.; Jiang, L. 3D Anisotropic Au@Pt-Pd hemispherical nanostructures as efficient electrocatalysts for methanol, ethanol, and formic acid oxidation reaction. *Adv. Mater.* **2021**, *33*, 2100713.

[175] Ding, J.; Liu, Z.; Liu, X. R.; Liu, J.; Deng, Y. D.; Han, X. P.; Zhong, C.; Hu, W. B. Mesoporous decoration of freestanding palladium nanotube arrays boosts the electrocatalysis capabilities toward formic acid and formate oxidation. *Adv. Energy Mater.* **2019**, *9*, 1900955.

[176] Rettenmaier, C.; Arán-Ais, R. M.; Timoshenko, J.; Rizo, R.; Jeon, H. S.; Kühl, S.; Chee, S. W.; Bergmann, A.; Cuenya, B. R. Enhanced formic acid oxidation over SnO_2-decorated Pd nanocubes. *ACS Catal.* **2020**, *10*, 14540–14551.

[177] Ye, W.; Chen, S. M.; Ye, M. S.; Ren, C. H.; Ma, J.; Long, R.; Wang, C. M.; Yang, J.; Song, L.; Xiong, Y. J. $Pt_4PdCu_{0.4}$ alloy nanoframes as highly efficient and robust bifunctional electrocatalysts for oxygen reduction reaction and formic acid oxidation. *Nano Energy* **2017**, *39*, 532–538.

[178] Ding, J.; Liu, Z.; Liu, X. R.; Liu, B.; Liu, J.; Deng, Y. D.; Han, X. P.; Hu, W. B.; Zhong, C. Tunable periodically ordered mesoporosity in palladium membranes enables exceptional enhancement of intrinsic electrocatalytic activity for formic acid oxidation. *Angew. Chem.* **2020**, *132*, 5130–5139.

[179] Yan, Y. C.; Li, X.; Tang, M.; Zhong, H.; Huang, J. B.; Bian, T.; Jiang, Y.; Han, Y.; Zhang, H.; Yang, D. R. Tailoring the edge sites of 2D Pd nanostructures with different fractal dimensions for enhanced electrocatalytic performance. *Adv. Sci.* **2018**, *5*, 1800430.

[180] Xiong, Y.; Dong, J. C.; Huang, Z. Q.; Xin, P. Y.; Chen, W. X.; Wang, Y.; Li, Z.; Jin, Z.; Xing, W.; Zhuang, Z. B. et al. Single-atom Rh/N-doped carbon electrocatalyst for formic acid oxidation. *Nat. Nanotechnol.* **2020**, *15*, 390–397.

[181] Lu, Y. Z.; Zhang, C. M.; Li, X. K.; Frojd, A. R.; Xing, W.; Clayborne, A. Z.; Chen, W. Significantly enhanced electrocatalytic activity of Au_{25} clusters by single platinum atom doping. *Nano Energy* **2018**, *50*, 316–322.

[182] Zhang, Z.; Gong, Y. Y.; Wu, D. B.; Li, Z.; Li, Q.; Zheng, L. W.; Chen, W.; Yuan, W. Y.; Zhang, L. Y. Facile fabrication of stable PdCu clusters uniformly decorated on graphene as an efficient electrocatalyst for formic acid oxidation. *Int. J. Hydrogen Energy* **2019**, *44*, 2731–2740.

[183] Wen, X. L.; Yin, S.; Yin, H. M.; Ding, Y. A displacement dealloying route to dilute nanoporous PtAu alloys for highly active formic acid electro-oxidation. *Electrochim. Acta* **2021**, *373*, 137884.

[184] Duchesne, P. N.; Li, Z. Y.; Deming, C. P.; Fung, V.; Zhao, X. J.; Yuan, J.; Regier, T.; Aldalbahi, A.; Almarhoon, Z.; Chen, S. W. et al. Golden single-atomic-site platinum electrocatalysts. *Nat. Mater.* **2018**, *17*, 1033–1039.

[185] Liu, L. C.; Corma, A. Metal catalysts for heterogeneous catalysis: From single atoms to nanoclusters and nanoparticles. *Chem. Rev.* **2018**, *118*, 4981–5079.

[186] Wang, Y.; Zheng, X. B.; Wang, D. S. Design concept for electrocatalysts. *Nano Res.* **2022**, *15*, 1730–1752.

[187] Jing, H. Y. ; Zhu, P. ; Zheng, X. B. ; Zhang, Z. D. ; Wang, D. S. ; Li, Y. D. Theory-oriented screening and discovery of advanced energy transformation materials in electrocatalysis. *Adv. Powder Mater.*, in press, https://doi.org/10.1016/j.apmate.2021.10.004.